UNIVERSITY OF CAPE TOWN

DEPARTMENT OF PHYSICS

ENERGY CORRELATIONS OF PROMPT NEUTRONS FROM ^{252}Cf FISSION

D.M. WHITTAL

Thesis submitted in partial fulfilment of
the requirements for the degree of

MASTER OF SCIENCE

in the Faculty of Science

May 1983

ABSTRACT

Measurements have been made of the neutron-neutron energy correlations for coincident neutrons emitted in the spontaneous fission of ^{252}Cf. The hypothesis that cooling of the fission fragments during the cascade evaporation of prompt neutrons affects the energies of successive neutrons in a cascade has been investigated by a comparison of the energy correlations of coincident neutrons from the same fragment with those of coincident neutrons from opposite fragments in the same fission. It is found that the energies of coincident neutrons are positively correlated and that the correlation coefficient is greater for neutrons from opposite fragments than for neutrons from the same fragment.

This provides a sensitive test of the nature of neutron emission in an evaporation cascade. The energy correlations of random (non-coincidental) neutrons have also been investigated and are found to show similar but smaller correlation trends.

It is concluded that there is some evidence for the cascade cooling effect on the energies of prompt fission neutrons.

ACKNOWLEDGEMENTS

I express my appreciation and gratitude to:

Professor F.D. Brooks, who supervised this work, for his tireless assistance with the experimental work, his ever-resourceful encouragement with the data analysis, and the difficult task of guiding me through the writing of this thesis by long-distance communication, during the period for which I was in Pretoria;

Dr J.B. Clark and Dr S. Hart of the National Institute for Materials Research, for their encouragement, and for allowing me the time and the facilities to complete this work;

The Council for Scientific and Industrial Research for their financial assistance;

The scientific and technical staff of the Southern Universities Nuclear Institute, for assistance with the experimental work;

Mr S. Allie and Mr B.R.S. Simpson, who assisted with some of the computing and experimental work;

Mrs J.K. Turnbull and Mrs U.A. Sharp of the National Physical Research Laboratory, for drawing most of the diagrams;

My mother for her support of my studies;

Alix for her patience and moral support;

Miss M.S. Taverner for typing the manuscript.

CONTENTS

CHAPTER 1

INTRODUCTION

The intriguing phenomenon which was later to be called "nuclear fission" was observed as early as 1935, just three years after the discovery of the neutron, but it was not until 1939 that Hahn and Strassmann (Ha39) were able to prove that isotopes of medium-weight elements were produced in the bombardment of natural uranium with slow neutrons. Within a year, Bohr and Wheeler (Bo39) had developed the liquid drop model, which pictures the fission of a nucleus as a process analogous to the division of a charged liquid drop. This model is still a cornerstone of fission theory and successfully explains many of the observed features of fission, with the notable exception of the strikingly asymmetric mass split.

A major contribution to fission theory was made by A. Bohr (Bo56), who combined the liquid drop model with the shell model to form the "unified model" of fission. According to this model, the conversion of excitation energy into potential energy of deformation results in a "cold" transition nucleus at the saddle point. The spins and parities of the few widely spaced quantum states available thus have a marked effect on the mode of fission. The more general inclusion of shell effects in spherical and deformed nuclei by Strutinsky (St67, St68) was an important development in the theory of fission. However, an adequate theoretical description of fission still presents a formidable task to the theoretician.

Investigation of the highly excited neutron-rich fragment nuclei, produced by the fission process, is of particular interest because of the insight that can be gained into the behaviour of nuclei far from the line of

stability, and because these nuclei are vectors of information on the fission process itself. De-excitation of these nuclei takes place primarily through the prompt emission of excess neutrons, followed by gamma ray emission.

The evaporation model for fission fragment de-excitation and the concept of a nuclear temperature (We37) have long provided the basis upon which analysis and models of fission neutron spectra have been founded. There are obvious advantages in being able to apply the formalism of a well-developed theory, namely classical thermodynamics, to a less well-understood, but analogous problem (fission), but it should be borne in mind that *"both nuclear fission itself and neutron emission from fission fragments are very complex processes and the simplifications that arise out of this complexity have only a limited range of validity"* (Kl72). For instance, the evaporation model, which pictures the fission fragments simply as spherical "hot" bodies, makes no provision for shell effects on the de-excitation of these nuclei. Nevertheless, the overall picture of neutron emission from fission fragments is still based upon thermodynamical analogies: the excitation energy of the nucleus is expressed in terms of a nuclear temperature and the subsequent expulsion of particles is analogous to an evaporation process.

However, twenty years since the publication by Bowman *et al.* (Bo62, Bo63) of the first comprehensive analysis of prompt neutrons from ^{252}Cf spontaneous fission, it is still not known how well the energies of more than one neutron from the same fragment conform to the predictions of the evaporation model, nor to what extent such factors as shell effects and angular momentum affect emission at high excitation energies.

Further information on the mechanism of neutron emission from the highly excited fission fragments may be gained from the measurement of energy correlations of these neutrons, which is the subject of the present investigation.

1.1 THE EVAPORATION MODEL AND THE ^{252}Cf SPECTRUM

Statistical methods (We37) may be applied to the calculation of the de-excitation of fission fragments because of the extremely small energy-level spacing at the high excitation energies in which these heavy nuclei are formed. In particular, thermodynamical analogies imply that, for a nucleus of given excitation energy and nuclear temperature, the energy of an emitted neutron is drawn from a spectrum, the mean energy of which is determined by the nuclear temperature. However, each neutron emitted in an evaporation cascade, in removing excitation energy from the parent fragment, causes a substantial drop in its nuclear temperature. Thus, if two neutrons are observed from one and the same fragment, they would be drawn from evaporation spectra of two different temperatures. In other words, the energies of neutrons emitted from the same fragment might be expected to be anti-correlated, with some preference for low energy accompanying high energy.

It was pointed out some time ago (Te59) that the assumption of a single temperature for the fission spectrum did not fully represent the situation on the Weisskopf picture. Smith *et al.* (Sm57) used a distribution of estimated *residual* excitation energies (after the emission of one neutron) to predict the average

spectrum of the second neutron in an evaporation cascade. Terrell (Te59) devised a method to obtain an average nuclear temperature from a combination of distributions representing initial excitation energy and residual excitation energies (after the emission of one or more neutrons). Assuming that the neutrons in the fission fragment centre-of-mass system are emitted in a Weisskopf evaporation spectrum (We37), Terrell's method gives rise to a Maxwellian spectrum for the neutron energies in the laboratory frame, of form:

$$N(E) = C \sqrt{E} \exp(-E/T_m)$$

where C is a normalising constant and T_m is related to the average neutron energy, $\bar{E}$, by the equation $T_m = {}^2/_3 \bar{E}$. T_m is not, however, the nuclear temperature, since the derivation of the Maxwellian shape is somewhat unphysical; it just happens to describe very well the shape of the spectrum which results from a combination of evaporation spectra of different nuclear temperatures. In Terrell's own words, *"This is no doubt a fortuitous result .... It is, however, a fortunate result because of the simple properties of this one-parameter distribution and the ease with which it may be fitted to experimental data."*

Watt (Wa52) derived an alternative distribution for the energies of neutrons in the laboratory frame, assuming the centre-of-mass distribution to be Maxwellian, but preference for a modified Maxwellian spectrum has overshadowed it in recent years. Bowman and co-workers (Bo62), for instance, obtained a reasonably good fit to their data by employing a three-component (i.e. three T-parameters)

Maxwellian spectrum, in the fragment rest frame, in order to allow for the spread in initial excitation energies of the fragments and for the decreases in excitation energy during cascade cooling. In a review paper, Kluge (Kl72) observes that *"until recently the best theoretical established spectrum form is the Maxwellian one."* Bowman *et al.* (Bo63) found that, over a wide range of mass divisions and excitation energies, a standard Maxwellian *shape* could be assumed for the distributions of neutron energies, even though the average energies of these distributions could be very different.

Nevertheless, the Maxwellian spectrum is only an approximation to the true neutron energy spectrum. In particular, several authors (Sm57, Me67, Gr73) have observed an excess of low energy neutrons (<0,7 MeV) in measured spectra in comparison with a Maxwellian spectrum. At high energies, too, there appear to be discrepancies (We72, Gr73), the experimentally determined yield of neutrons >8 MeV being less than would be expected for a Maxwellian distribution (see Figure 1.1). Meadows (Me67) suggested that the most probable cause of these discrepancies was anisotropic emission of neutrons from the fission fragments. Models which include anisotropic emission in the centre-of-mass frame of the fragment, with enhanced emission along the fission axis, fit the data rather well (Te59, Me67, Gr73). The existence of a small component of scission neutrons, i.e. neutrons emitted isotropically in the laboratory frame, at the instant of scission of the fissioning nucleus, has also been proposed (Bo62, Sk63, Ka63). Estimates of this component in ^{252}Cf fission vary from zero (Sk73) to 25% (Gr73) of prompt neutrons, but the existence of scission neutrons has yet to be conclusively demonstrated experimentally. A discussion of the scission neutron question is to be found in Pringle's Ph.D. thesis (Pr77).

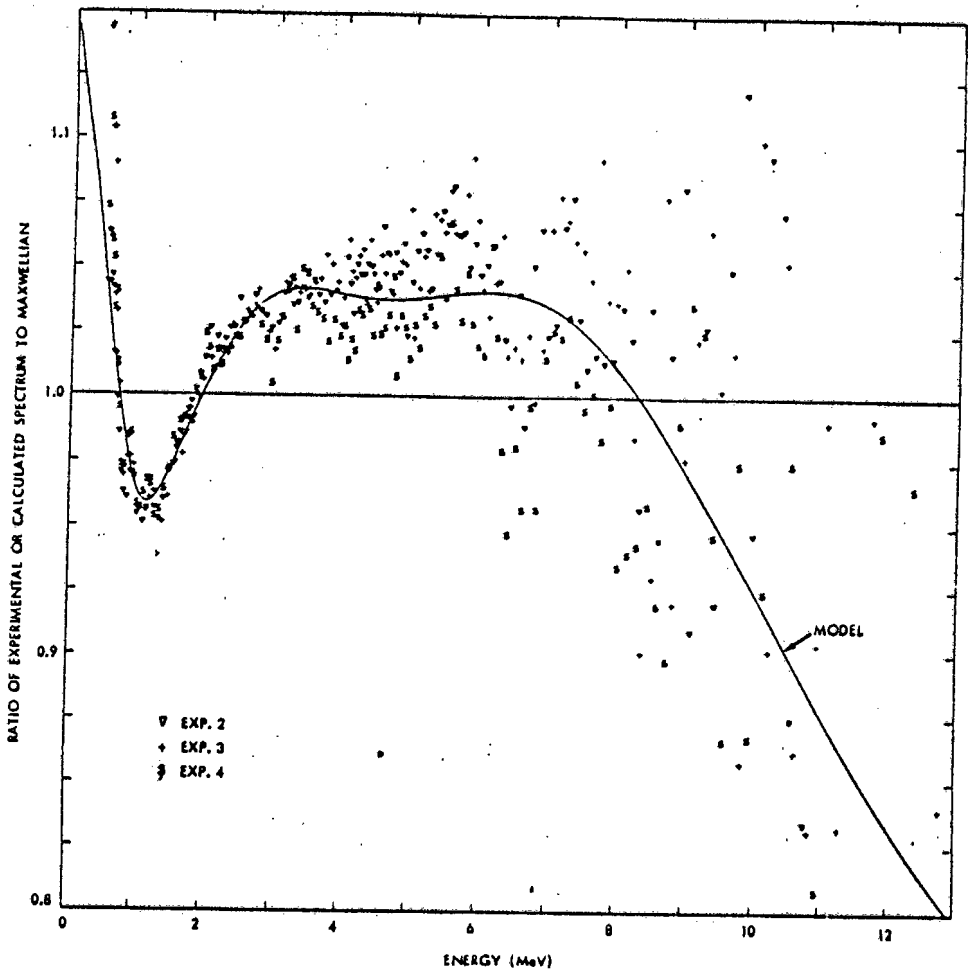

Figure 1.1: A comparison between the measured neutron spectrum from ^{252}Cf fission and a Maxwellian spectrum. Data points are ratios of the experimental values to the Maxwellian values. The curve shows the prediction of a model developed to fit the data. (Figure from Gr73).

The numerical results of "exact" cascade calculations also seem to reproduce the experimentally observed spectra quite well. One of the first such calculations was that of Kluge (Kl71), but his calculated fission spectra compared poorly with experimental data *"due to the neglect of the spread in initial fragment excitation energies."* Browne and Dietrich (Br74) performed a more detailed

calculation of the ^{252}Cf neutron spectrum, using the Hauser-Feshbach formalism, in which experimental information was used to determine such parameters as fragment excitation energies and spin distributions, but no arbitrary parameters were introduced into the calculation to produce a fit to the data. However, the method is sufficiently complicated that it is difficult to apply it to the full range of possible fragments and excitation energies without making averaging approximations. Nevertheless, their results compare well with experimental data (see Figure 1.2).

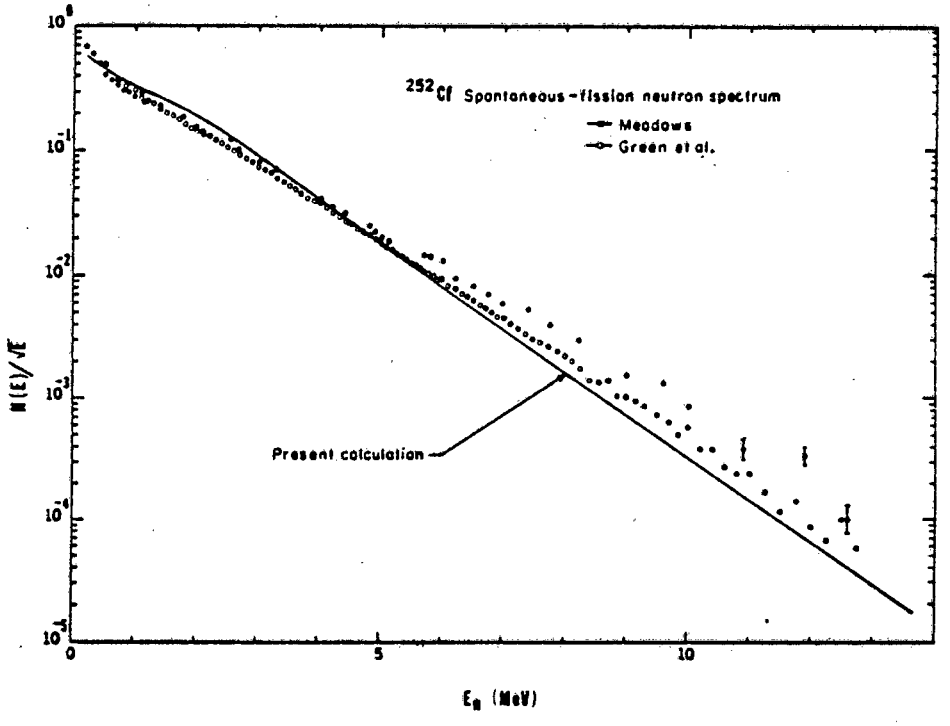

Figure 1.2: Experimental and calculated neutron spectra (laboratory energy) for ^{252}Cf fission. The solid line represents the results obtained from a Hauser-Feshbach calculation; the points represent the data of Meadows (Me67) and Green *et al.* (Gr73). N(E) is normalised so that the integral of N(E) is equal to one. (Figure from Br74).

In a recent calculation, Madland and Nix (Ma82) used standard nuclear-evaporation theory to calculate prompt neutron spectra for, amongst others, ^{252}Cf spontaneous fission. They avoided the complexity of an "exact" cascade calculation, but at the same time included the cascade effect by using the triangular-shaped residual nuclear temperature distribution derived by Terrell (Te59). An important feature of their calculation was the way in which they allowed for the variation in initial fragment excitation energy by calculating energy-dependant compound-nucleus cross sections for representative mass divisions and interpolating between the calculated values in order to estimate the distribution of initial excitation energies as a function of all mass divisions. The neutron spectra thus calculated compare well with experimental data (see Figure 1.3).

Another approach to the calculation of prompt fission neutron spectra is the Monte Carlo method, in which the statistical nature of neutron emission from fission fragments is exploited in a computer simulation of the process. This method will be discussed more fully in Chapter 4. Pringle and Brooks (Pr75, Pr77) used Monte Carlo simulations to assess the effect on the neutron spectrum of various forms of anisotropic emission, and scission components, but a more complex modelling procedure would be necessary to produce accurate simulated spectra for meaningful comparison with experimentally determined spectra. Franklyn *et al.* (Fr78) used a slightly different Monte Carlo simulation to generate a fission-neutron energy spectrum for ^{235}U which is in close agreement with measured spectra except at energies below 1 MeV, where it underestimates the measured

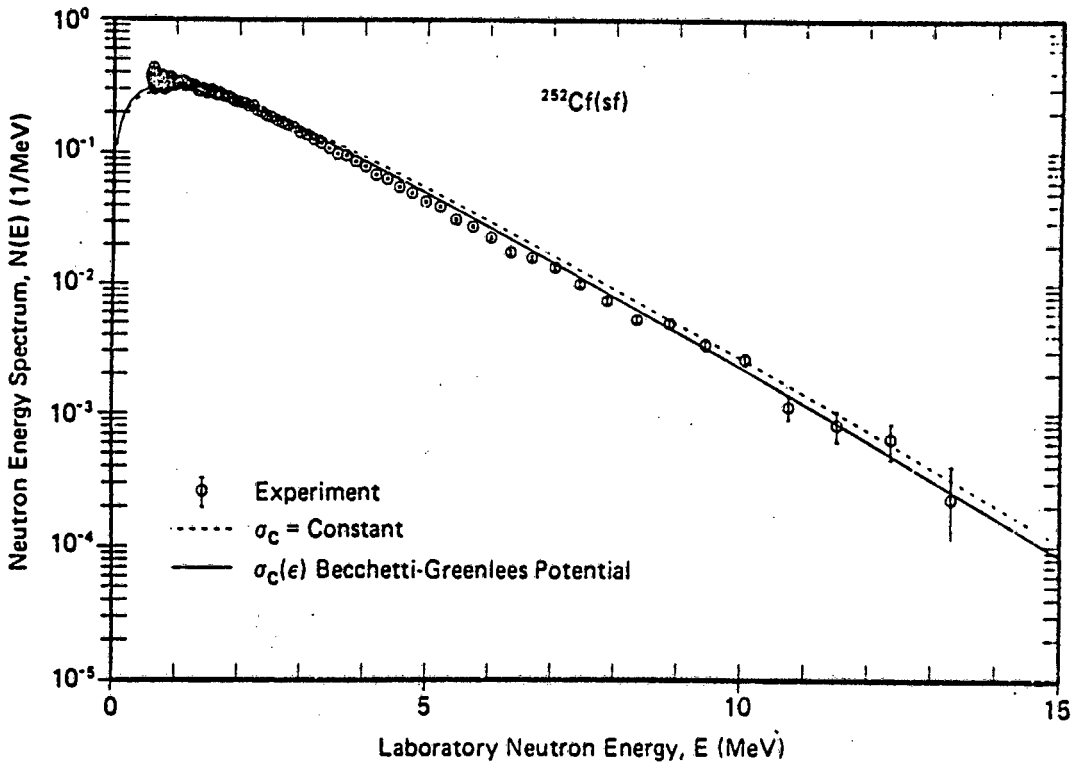

Figure 1.3: Comparison between the neutron spectrum (laboratory energy) for ^{252}Cf fission, calculated by Madland and Nix, and the experimental data of Boldeman *et al.* (Bo79). The solid curve represents the spectrum calculated by using energy-dependant compound-nucleus cross sections and fits the experimental data better than the dashed curve, which is the spectrum obtained when a constant cross section is used. (Figure from Ma82).

distribution (see Figure 1.4). Kildir and Aras (Ki82) were able to reproduce mass and charge distributions, and they also calculated $\bar{\nu}(A)$, the average number of prompt neutrons as a function of fragment mass, in good agreement with the experimental values, but they did not develop their Monte Carlo model far enough to enable them to produce neutron spectra. The simulation took into account the

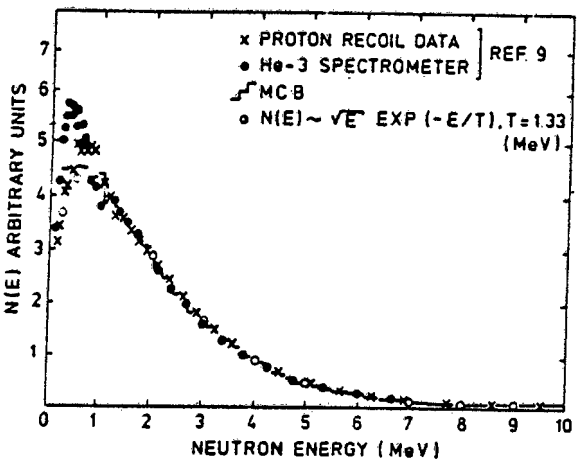

Figure 1.4: A comparison of the Monte Carlo simulation (histogram) of Franklyn *et al.* (Fr78) with experimental data and a Maxwellian distribution (open circles). (Figure from Fr78).

effect of cascade cooling of the fission fragments during neutron emission. Generally, there is great interest in pursuing this line of approach to the calculation of fission neutron spectra; it is very flexible and many millions of fission histories can be simulated in a short time on any modern computer, so that statistical accuracy never presents a problem.

To summarise, it appears that, whether a Maxwellian or Watt spectrum is fitted to experimental data, or whether a neutron spectrum is calculated by any of the abovementioned methods, better agreement with experimentally determined spectra is obtained when the cascade cooling phenomenon is taken into account. Considering the success with which nuclear-evaporation theory has been applied to the interpretation of fission phenomena, and the fact that cascade cooling of excited nuclei is a logical corollary to this theory, it is hardly surprising that it is becoming standard practice to include cascade cooling considerations in calculations or models of the

fission fragment de-excitation process. However, the existence of this effect *has yet to be experimentally demonstrated.* On the contrary, Gavron and Fraenkel (Ga74) concluded from the analysis of their data that there was no correlation of evaporation energies of two neutrons in an evaporation cascade, nor was there a correlation between the excitation energy of the fragment and the average kinetic energy of the neutrons, in the fragment centre-of-mass frame. Parameters which they obtained from their experimental results included: $\langle\eta\rangle^{(1)}$, the average neutron energy, in the centre-of-mass frame of the fragment, for events in which only one neutron was detected; $\langle\eta\rangle^{(2)}$, the average energy for events in which two neutrons were detected; and $\langle\eta_1\eta_2\rangle^{(2)}$, the average of the product of the centre-of-mass energies of two neutrons emitted from the same fragment. They found that

$$\langle\eta\rangle^{(1)} = \langle\eta\rangle^{(2)}, \quad \text{and}$$

$$\{\langle\eta\rangle^{(2)}\}^2 = \langle\eta_1\eta_2\rangle^{(2)}.$$

Their discussion of these findings includes the following:

"These results have no simple explanation. If the total excitation energy E_x was constant in a given nucleus we would expect a negative correlation between η_1 and η_2, the c.m. kinetic energies of neutrons "1" and "2" in the cascade. This is because an increase in η_1 leaves less excitation energy for the emission of the second neutron. However, if E_x varies we would expect η_1 to increase as E_x increases. Thus an increase in η_1 implies an increase in the total initial excitation energy which in turn causes an increase in the kinetic

energy of all the neutrons. Thus the experimental lack of correlation between two neutrons could be explained by the existence of two correlation mechanisms which cancel each other. It is, however, most surprising that this cancellation exists in the entire range of fragment masses and excitation energies.

We have no explanation for the lack of correlation between the average kinetic energy and the total excitation energy. Fragments emitting one neutron on average should exhibit relatively high neutron c.m. kinetic energies when two neutrons are detected. Evaporation calculations show that an 0.1-0.2 MeV difference should be observed. In practice, the observed difference is an order of magnitude smaller (∿ 1%) and could be due to recoil effects, dispersion effects, etc."

It appears that no-one other than Gavron and Fraenkel has ventured to draw any conclusions, from experimental results, about the existence (or non-existence) of these correlation effects, which are assumed to be present by those who develop models to describe fission fragment de-excitation. Since the conclusions drawn by Gavron and Fraenkel are contrary to what might be expected, it is of interest to investigate this matter further. The aim of this work was thus to investigate the energies of prompt neutrons which were known to have been emitted from the same fission fragment, in order to determine whether or not they were in any way correlated. The results of such an investigation would test the "cascade cooling" hypothesis directly, and indirectly shed some light upon other aspects of the fission process.

1.2 DESIGN OF THE EXPERIMENT

The most practical way to measure neutron energies accurately is by the time-of-flight technique. For this purpose, it was decided to use two liquid scintillators to detect coincident neutrons (by proton recoil in the scintillators). Since a relatively strong encapsulated source of ^{252}Cf was to be used as the spontaneous-fission source, a thin plastic scintillator was placed near the source to record the "start" of the time of flight by detecting a fission γ-ray or neutron. The apparatus is described in more detail in Chapter 2. Since the fragments themselves would not escape from the source, the measurements would be averaged over all orientations of the fission axis, and some method had to be devised whereby coincident neutrons from the same fragment could be distinguished from coincident neutrons from opposite fragments.

It is appropriate, at this stage, to discuss the angular distribution, in the laboratory frame, of the prompt neutrons emitted by the accelerated fission fragments. Bowman *et al.* (Bo62) measured the angular distribution of neutrons, relative to the fission axis (see Figure 1.5).

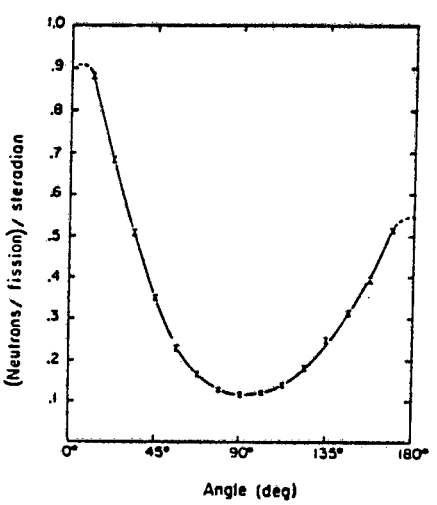

Figure 1.5: The measured angular distribution (laboratory frame) of neutrons from ^{252}Cf, relative to the fission axis, with the light fragment along 0° and the heavy fragment along 180°. (Figure from Bo62).

Apart from some discrepancies at small angles, and the inclusion of a small component ($\sim$ 10%) of scission neutrons, their results were by and large consistent with isotropic evaporation from the moving fragments. The translational motion of the fully accelerated fragments, which varies from $\sim$ 0,8 cm/ns for the heaviest fragments to $\sim$ 1,6 cm/ns for the lightest (Wh63), results in the distribution of neutrons in the *laboratory* frame being sharply peaked in the direction of motion of the fragments. It can be seen in Figure 1.5 that the effect is more pronounced in the case of neutrons from the light fragment, as may be expected from the fact that it is faster than the heavy fragment and thus contributes a greater component to the laboratory velocities of the neutrons which it emits. It was thus decided to make a comparison between the energies of coincident neutrons emitted:

(a) at a small relative angle ($\sim$ 30°) to one another; and
(b) at a relative angle of 180° to one another.

These two geometries would select *predominantly:*

(a) two neutrons from one of the fragments only (at 30°); or
(b) one neutron from each fragment (at 180°),

with the fission axis mostly pointing towards the detectors, as illustrated schematically in Figure 1.6. If, as some authors believe, emission in the centre-of-mass frame of the fragment is indeed anisotropic, with peaking along the fission axis, the phenomenon would be advantageous to this experiment if one considers the design.

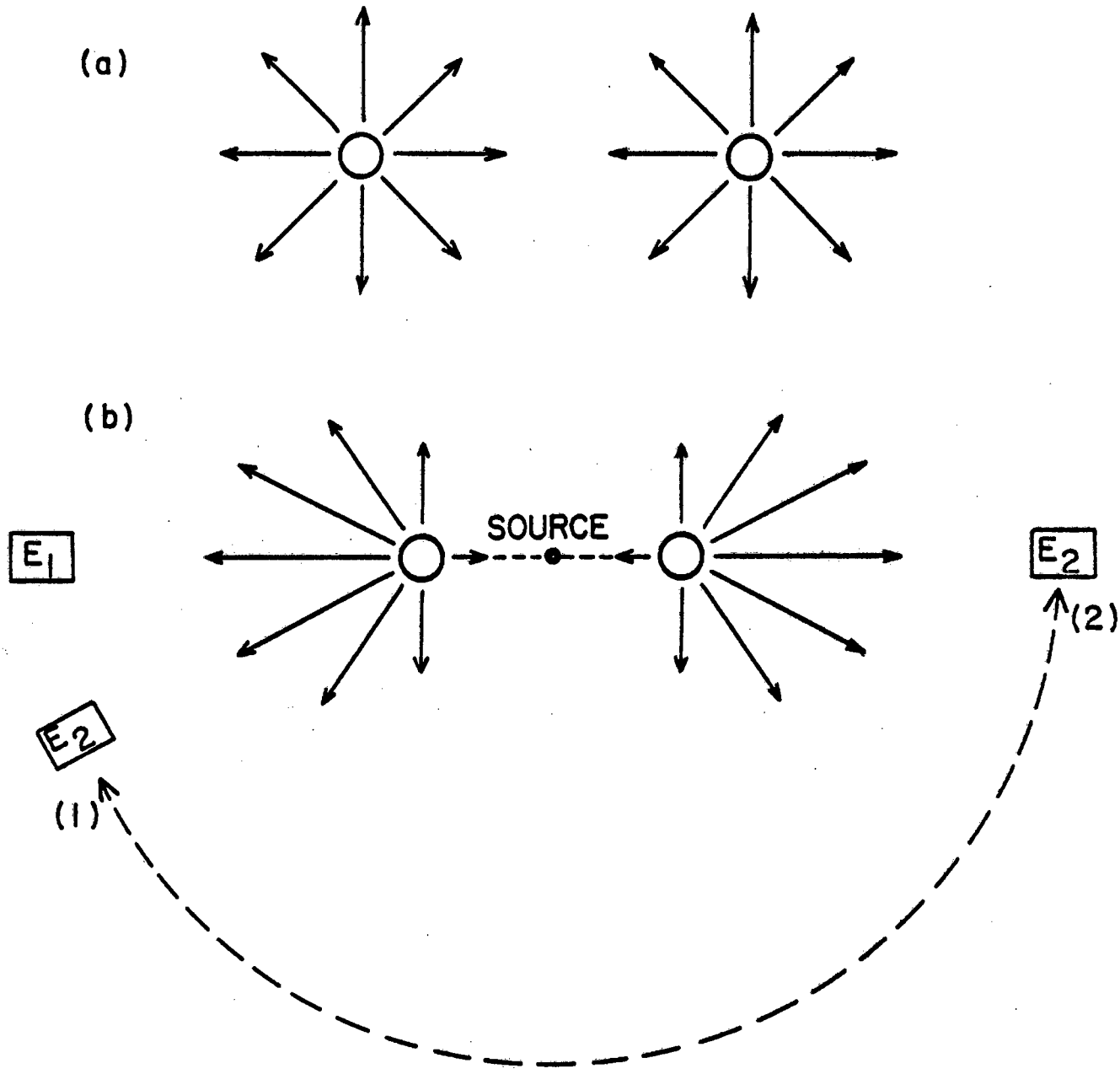

Figure 1.6: Schematic representation of the experimental configuration. The arrows in (a) represent the velocities of neutrons emitted isotropically in the rest frames of the fragments, with average energy 1,4 MeV in these frames (Bo62), which implies a velocity of 1,7 cm/ns. The arrows in (b) represent the velocities of these neutrons in the laboratory frame, assuming an average fragment velocity of 1,2 cm/ns (Bo63).

With the detectors in configuration (1), coincident neutrons originating predominantly from the *same* fragment are recorded; at (2), coincident neutrons originating predominantly from *opposite* fragments are recorded.

Supposing that the fission axis were always to point towards the detectors, identification, by the above approach, of neutrons from the same fragment or from opposite fragments respectively, would be almost always correct. Feather and Vass (Fe75) have calculated that the ratio of the "backwards" spectrum (neutrons emitted opposite to the direction of motion of the fragment) to the "forwards" spectrum is of the order of 1:500. This is, of course, an idealised situation, since the fission axis can be at any angle to the detectors. In the worst case, when the fission axis is "broadside" to the detectors, as many pairs of coincident neutrons from the same fragment as from opposite fragments would be detected in either configuration. Fortunately for this experiment, "broadside" emission of *two* neutrons is of the order of forty times less likely than "forwards" emission of two neutrons (fission axis pointing towards the detectors), as can readily be appreciated from the angular distribution, Figure 1.5. It is reasonable to conclude, therefore, that the two detector configurations do, in fact, select coincident neutrons emitted predominantly from the same fragment, and from opposite fragments respectively. Thus, the comparison of the energy distributions observed at these two configurations would indicate whether or not a significant energy-energy correlation exists for neutrons emitted from the same fragment.

CHAPTER 2

EXPERIMENTAL METHODS

2.1 OUTLINE OF EXPERIMENTS

The experimental work was conducted at the Southern Universities Nuclear Institute (SUNI) during four independent run periods of 7 - 15 days each. A relatively strong source ($\sim$27 μg ^{252}Cf) was used for the first two runs, but the rate of accidental coincidences was unacceptably high. Because of this, a much weaker source ($\sim$0,5 μg) was used for the last two runs, and the results from only these two runs are presented here.

For the sake of brevity, the experimental configuration in which the two neutron detectors are at a small relative angle ($\sim$30°) to each other, will henceforth be called the "30° configuration"; similarly, the other configuration, in which the detectors are opposite each other, will be called the "180° configuration". The system was designed to alternate automatically between these configurations. The time-of-flight of each of the two coincident neutrons was recorded on buffer tape by the multiparameter data acquisition system. The energies of the corresponding recoil protons were also recorded. The fifth parameter to be recorded was a tag on the experimental configuration which made it possible for the data to be sorted later into a "30° configuration" set and a "180° configuration" set.

2.2 ^{252}Cf SOURCES

The primary decay mode for Californium-252 is α-particle emission; spontaneous fission accounts for only 3,1% of all disintegrations (Am72), and the combined "effective" half-life is 2,64 years (Sp74).

Each fission event results in an average of 3,773 ± 0,007 neutrons (Sp82) with average laboratory energy of 2,15 MeV (Bo74), plus about eight gamma photons which remove an average total of 7,0 ± 0,3 MeV of energy from the fission fragments (Sk80). Fission neutrons were emitted from the 0,5 μg source at a rate of about $1,2 \times 10^6$ n/s.

Both of the sources used were encapsulated, the 27 μg in stainless steel, and the 0,5 μg in a platinum-iridium container 18 mm long and 1 mm in diameter. Thus, only neutrons and γ-rays were present at the detectors. The type of fission source which makes fragment detection possible, usually an exposed coating of Cf_2O_3 on a suitable backing, is unfortunately too weak to provide reasonable count rates for the triple coincidence of two neutrons plus a fragment.

2.3 APPARATUS AND EXPERIMENTAL GEOMETRIES

The details of only the last two runs, i.e. Run 3 and Run 4, are described here.

The neutron detectors were NE-213 organic liquid scintillators in glass cylinders of dimensions 5,5 cm x 5,5 cm. A silicone fluid was used to couple them to the photomultiplier tubes (RCA 6655A's for Run 3 and RCA 8850's for Run 4), which were sheathed in μ-metal to provide magnetic shielding.

The time-zero detector consisted of a cylinder of thin (½-mm) plastic scintillator surrounding the source. The time of fission was signalled via a prompt fission gamma ray (or a neutron) detected by this plastic scintillator. Figure 2.1 illustrates the way in which the cylinder of scintillator was mounted on its photomultiplier tube (RCA 6342 for Run 3 and RCA 6655A for Run 4). In order to attenuate the high flux of low-energy gamma rays, mainly associated with the α-particle disintegrations, the "well" in which the Californium source was suspended, was lined with a 1 mm thick cylinder of lead, with a 2 mm thick disc at the base. The plastic scintillator rested in a groove in a perspex light-guide, which was

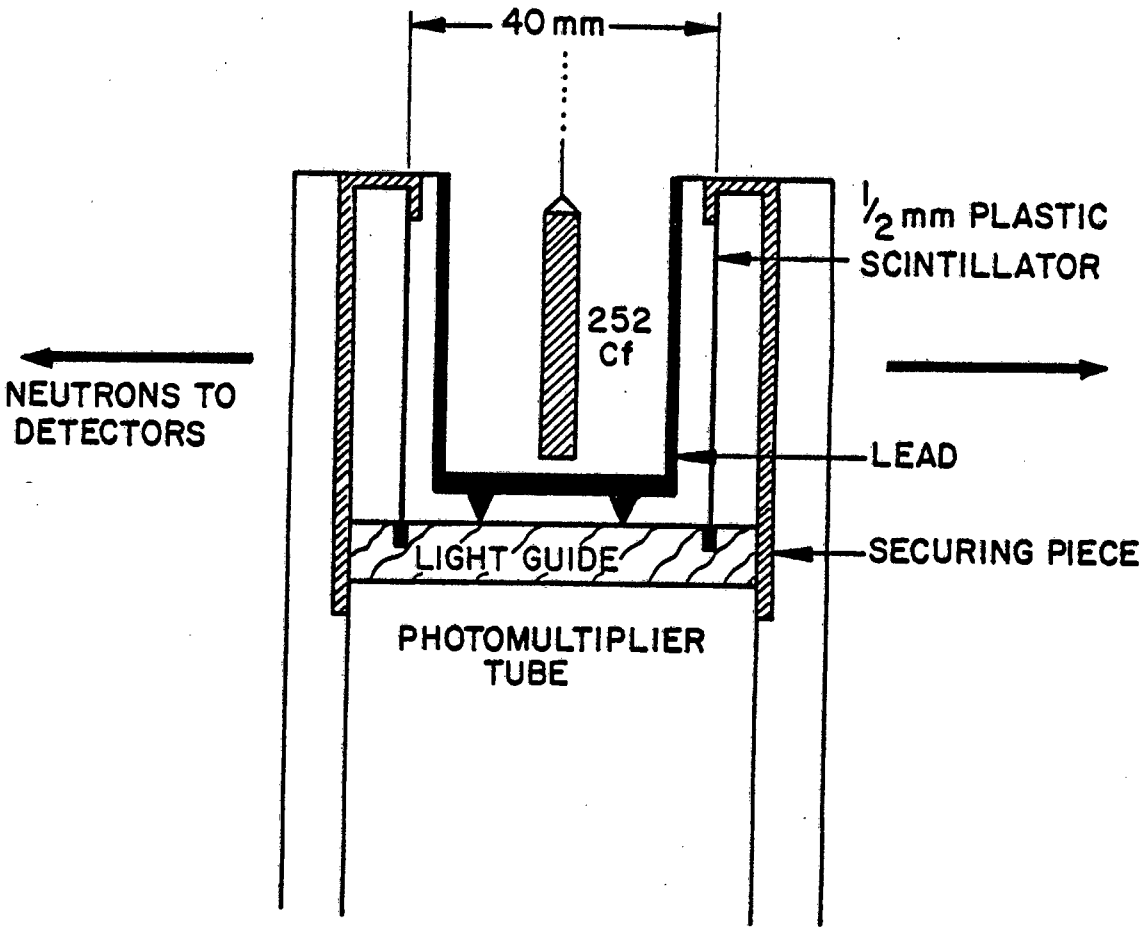

Figure 2.1: Construction of the time-zero detector. A cylinder of thin plastic scintillator surrounds the ^{252}Cf source.

optically coupled to the face of the photomultiplier tube in the usual way. Efficiency of light collection was improved in several ways:

(i) liquid paraffin in the groove ensured good optical coupling between the scintillator and the light-guide;

(ii) for optimal internal reflection within the light-guide, spacers separated its top surface from the bottom of the "well";

(iii) the aluminium surfaces on either side of the scintillator were painted with NE-560 diffuse reflector paint.

Scattering calculations indicate that less than 3% of the neutrons entering the liquid scintillators had been scattered from the perspex light-guide and less than 1% had been scattered in the plastic scintillator. Energy loss during scattering would naturally have resulted in many of these neutrons falling below the detection threshold, so the total recorded component of scattered neutrons from these objects was probably no more than $\sim$2% of all neutrons detected.

The experimental apparatus was mounted on a circular aluminium table, which was positioned in the middle of the neutron pit at SUNI, to maintain the maximum possible distance from any walls or other dense objects which might scatter neutrons towards the detectors. The time-zero detector was clamped in an upright position into a specially made aluminium stand in the centre of the table, with the Cf source suspended in the centre of the "well". The neutron detectors were supported in aluminium cradles in such a way that they lay in the

same horizontal plane as the Cf source (see Figure 2.2). The distances from the source to the middle of the liquid scintillators were 53,3 cm and 52,6 cm for Run 3 and Run 4 respectively. One detector was fixed in position, but the other was mounted on a mobile cradle attached to a rod which pivoted at the centre of the table. This detector could thus roll around from the 30° configuration to the 180° configuration, as illustrated in Figure 2.3. The system was automated so that it could alternate between the 30° and 180° configurations every few minutes during running periods lasting several hours. The comparison between results obtained in the two geometries was thereby freed of systematic errors which might have arisen from long-term drifts in the stability of electronic or other equipment. A remotely controlled DC motor was attached to the mobile cradle (see Figure 2.2). The drive wheel ran along the top surface of the table with a pincher roller on the underside, near the rim, to improve traction. Micro-switches on the rim of the table ensured that the detector assembly stopped at the correct position.

A shadow shield of borated wax was inserted between the two liquid scintillators in the 30° configuration (see Figures 2.2 and 2.3) to attenuate spurious coincidences arising from neutron scattering from one detector to the other. On the one hand, this "cross-talk" must be reduced as much as possible, but, on the other hand, too much scattering material in the vicinity of the liquid scintillators is undesirable. On the basis of Pringle's investigation into neutron attenuation in borated wax (Pr77), it was decided that a shadow shield of length 14 cm would be a good compromise between these considerations. In order to neutralise the effect of asymmetries in

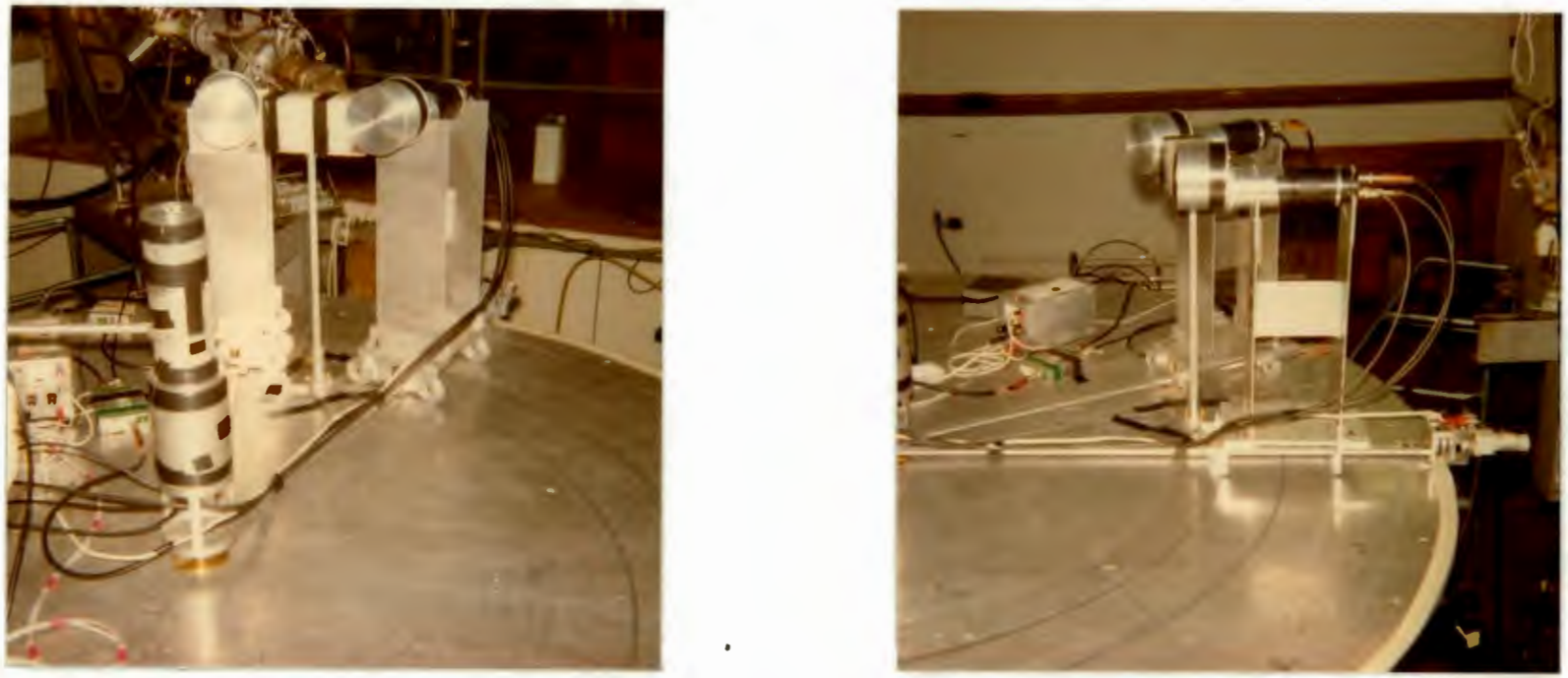

Figure 2.2: Two views of the experimental apparatus, with the neutron detectors in the 30° configuration.

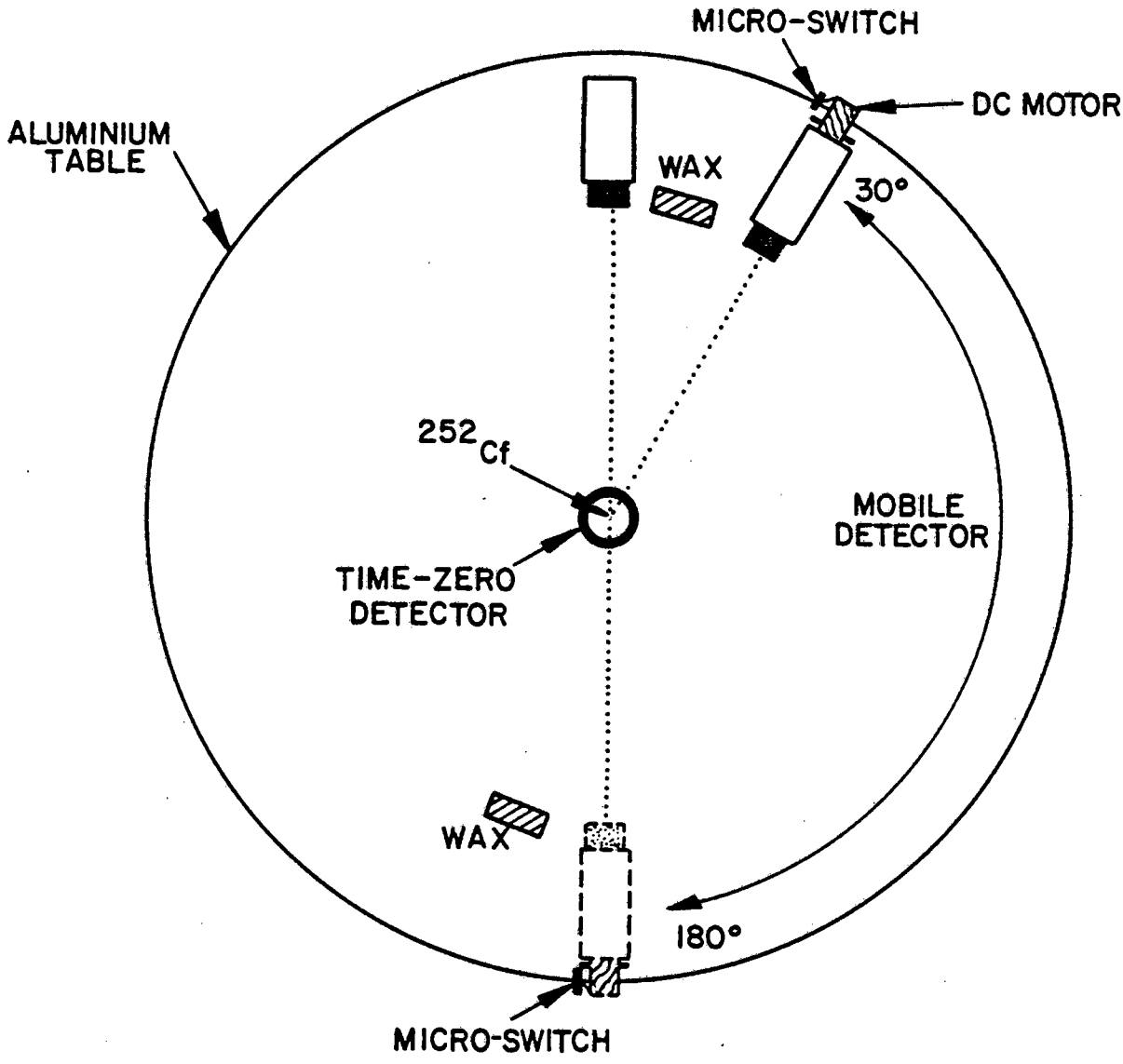

Figure 2.3: Top view of the experimental geometry. Most of the neutrons pass unimpeded through the aluminium walls of the "well" and when two are detected in coincidence, one in each liquid scintillator, their energies may be determined by time-of-flight.

the data caused by neutron scattering from the shadow shield, a "dummy" shadow shield of the same dimensions was placed at the 180° position.

2.4 ELECTRONIC CONFIGURATION

The main components of the electronic circuitry are illustrated schematically in Figure 2.4.

Pulse Shape Discrimination: The zero cross-over-timing technique for Pulse Shape Discrimination (PSD) (A161) was used to reject most of the gamma rays detected in the mobile scintillator. The PSD system on the fixed detector was more fundamental in its principle of operation: the "LINK PSD 5010" incorporates in a single, easily-tuned module the PSD method described by Adams and White (Ad 78), in which a comparison is made between the amount of light in the tail of a light-pulse and the total (integrated) light pulse. Unfortunately, only one of these systems was available at SUNI at the time of the experimental runs.

Time-of-flight: Because the count rate of the time-zero detector was 30 - 40 times that of the neutron detectors, the time-zero signal was delayed so that it could be used as the "STOP" inputs at the Time-to-Amplitude Converters, thus minimising the number of "false starts". The true "time" axis of the resultant distributions was consequently reversed with respect to the recorded TAC "pulse height" values, as shown in Figure 2.5.

Coincidence Gating: An "event" was recorded on buffer tape in multi-parameter mode only if a gate pulse was supplied by the Coincidence Logic circuitry. This required a time-of-flight measurement from each of the two neutron detectors in coincidence with signals from both PSD systems. Thus, almost all the recorded events were true

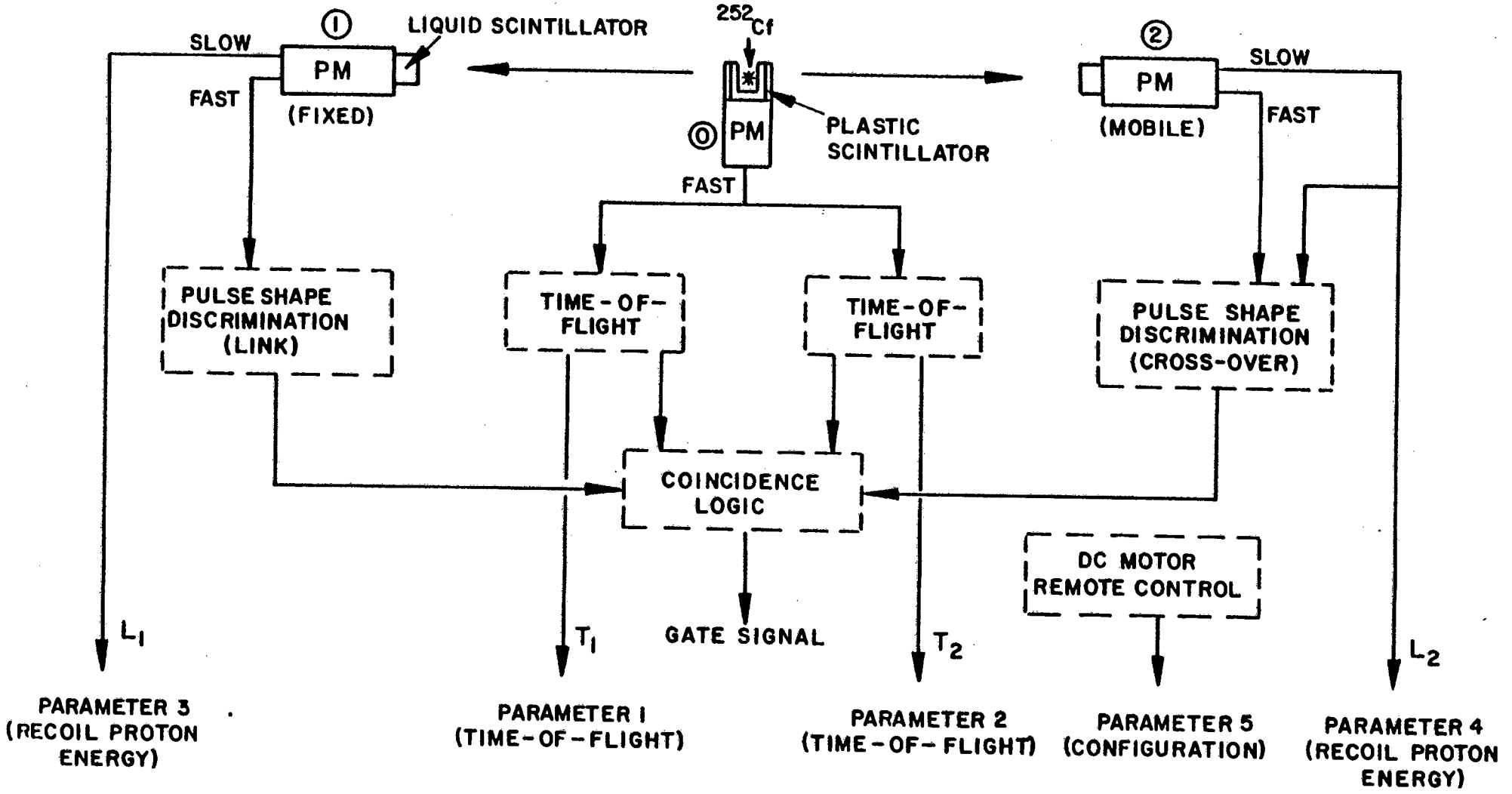

Figure 2.4: Schematic diagram of electronic configuration. γ-rays detected in the liquid scintillators are rejected by Pulse Shape Discrimination. A five-parameter "event" is recorded on buffer tape only when a gate signal is produced by the Coincidence Logic circuitry.

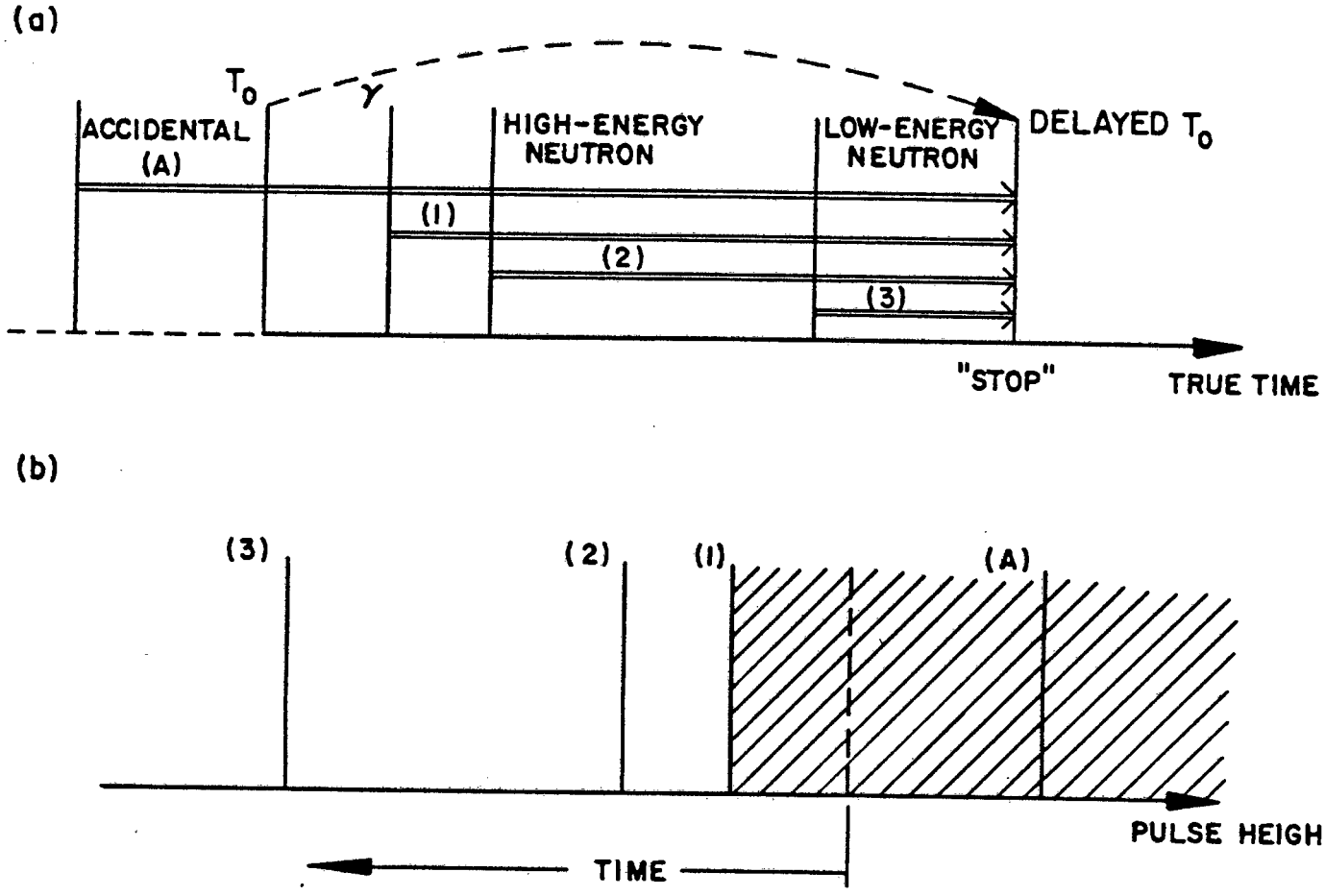

Figure 2.5: (a) The trigger from the time-zero detector, T_0, is delayed and becomes the "STOP" signal.

(b) The true time-of flight axis is reversed with respect to the Pulse Height axis. Any events represented by pulse heights in the shaded region are obviously "accidental" counts, since they represent "flight-times" shorter than those for gamma rays.

neutron-neutron coincidences, the exceptions being a small number of breakthrough gammas (PSD) and "accidental" counts (timing systems).

An Input Register supplied the data acquisition system with the "configuration" parameter. Bit 9 was set when the detectors were in the 30° configuration and Bit 10 was set when they were in the 180° configuration.

A detailed block diagram of the electronic circuitry is shown in Figure 2.6.

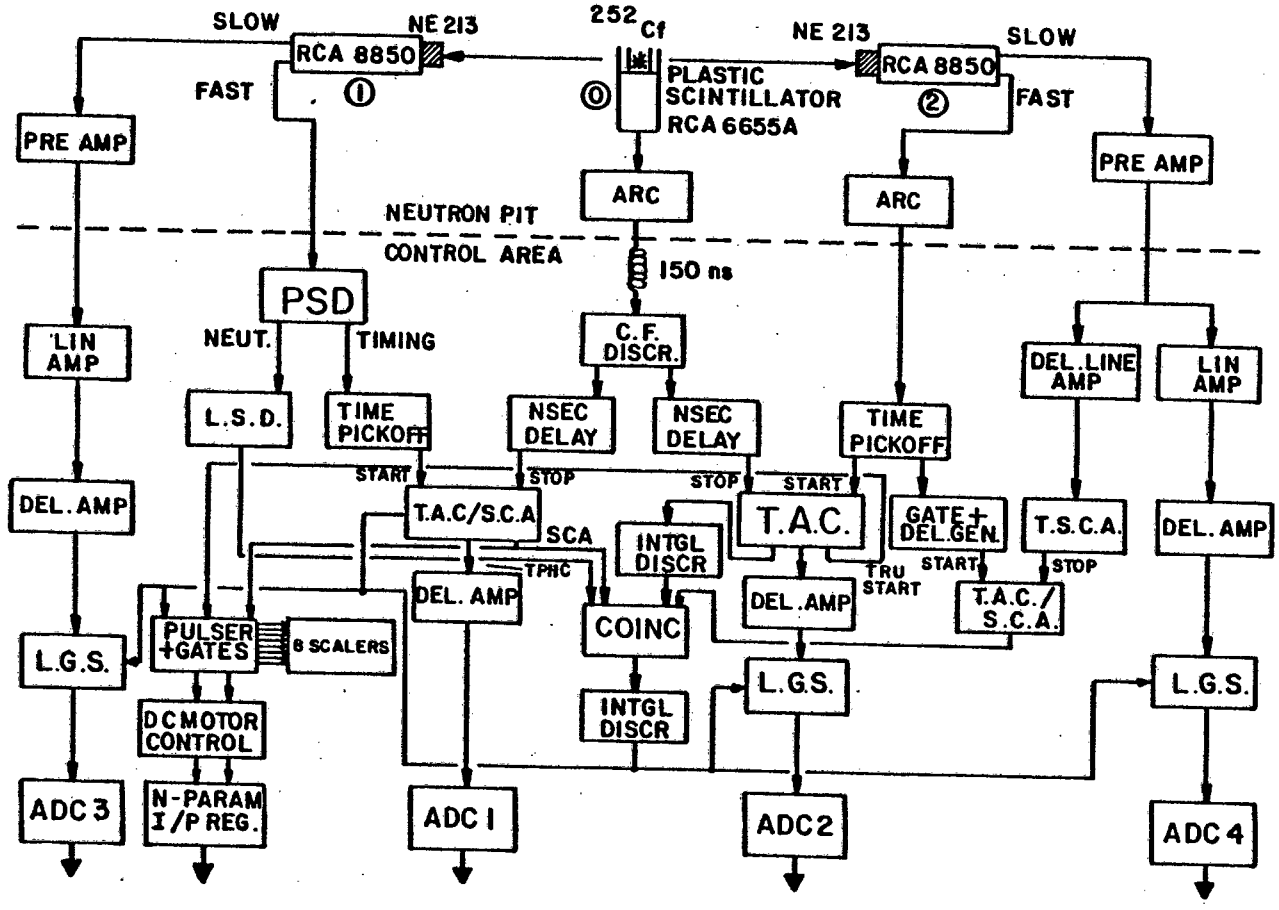

Figure 2.6: Block diagram of the electronic configuration. A PDP 15 computer stores the outputs of the ADC's on buffer tape.

Coincident neutron count-rates were typically 0,5 - 3/min., being very sensitive to PSD levels, which were always a compromise between losing too many low-energy neutrons and allowing too many break-through gamma rays.

The timing resulution was typically 4 - 5 nanoseconds.

2.5 CALIBRATIONS

The following calibrations were performed at least once during the course of each run:

(i) Time scale calibrations: the channel corresponding to time zero was determined in two independent ways. Firstly, a correction corresponding to the gamma ray flight-time was applied to the position of the γ-peak from ^{252}Cf. Secondly, the liquid scintillators were moved right up to the time-zero detector and the two back-to-back γ-photons from a ^{22}Na source were used to establish time zero on the time scale. The results of the two methods were in close agreement (<1%). The scale of each time parameter was determined by noting the shift in the position of the γ-peak (^{252}Cf or ^{22}Na) when a 50 ns calibrated delay-line was introduced into the circuitry at one of the TAC inputs. Agreement between ^{252}Cf and ^{22}Na results was <0,3%.

(ii) Gamma rejection: the ability of the PSD systems to reject gamma rays was tested by using a ^{60}Co source and comparing scaler readings with PSD "on" or "off". The zero cross-over-timing PSD system rejected 91% and 96% of γ-rays during Runs 3 and 4

respectively. Since the time-of-flight measurements enable further discrimination against γ-rays, it was decided not to improve this modest performance at the expense of low-energy neutrons. The "Link" system performed better, rejecting 99,3% (Run 3) and 99,9% (Run 4) of γ-rays without sacrificing a significant number of neutrons.

(iii) The recoil proton pulse height (the so-called L-parameter) "true zeroes" were found and the scales calibrated by noting the position of the ^{60}Co Compton electron edge for different gain settings of the Linear Amplifiers, and making use of scintillator response curves (Sm68, Cr70, Be71) to determine equivalent proton energy.

(iv) During the course of subsequent off-line analysis, the proton energy thresholds (with PSD) and neutron detection thresholds were found from density plots of proton pulse height (L) against neutron flight-time (T), as described by Pringle (Pr77). The process is illustrated in Figure 2.7. At the low energy (long time-of-flight) side of the density plot, the domain of "real" recoil protons is bounded by the threshold of the detector system (photomultiplier and PSD) and by a curve which represents neutron energy, i.e. maximum possible recoil proton energy. The neutron detection threshold is thus determined from the junction of these boundaries.

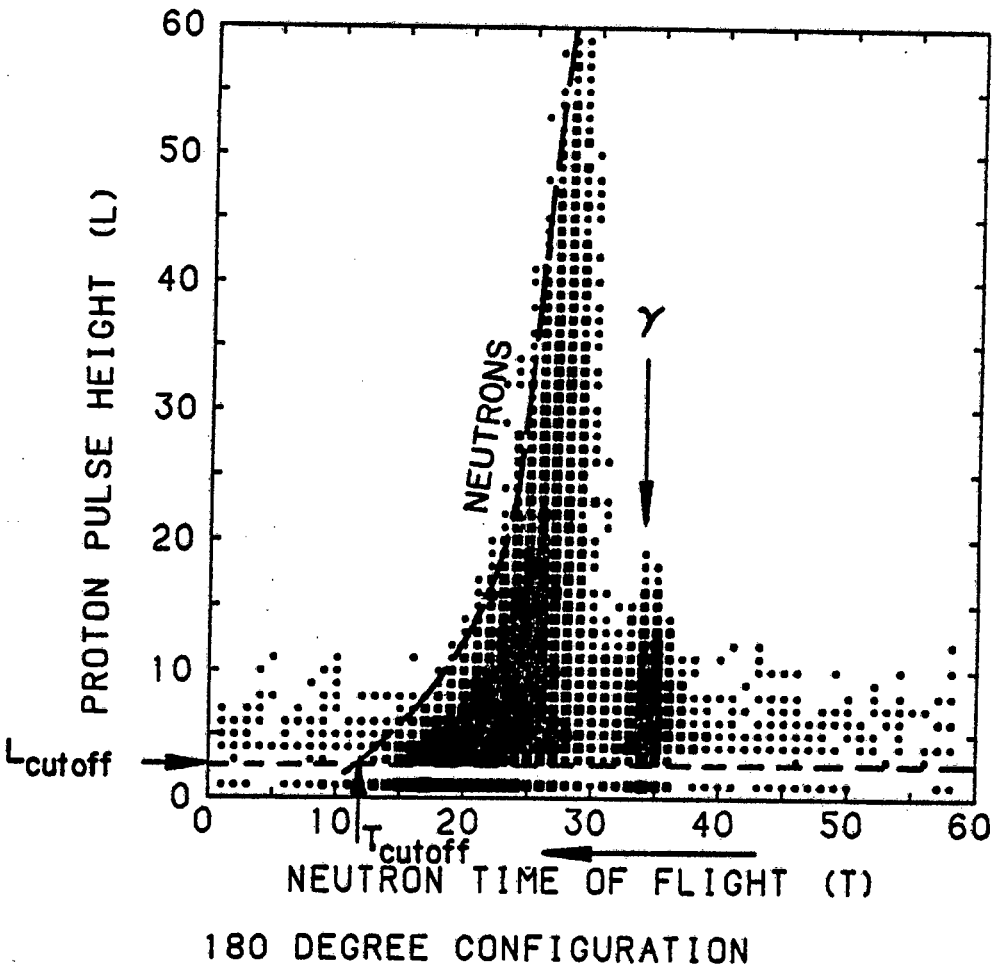

Figure 2.7: How a density plot is used to determine T_{cutoff} and thus the neutron detection threshold.

CHAPTER 3

ANALYSIS AND RESULTS

3.1 OUTLINE OF ANALYSIS

The multiparameter data stored on buffer tape were reduced on the UNIVAC computer at the University of Cape Town. Time-of-flight data were converted into their corresponding neutron energy values; various selection criteria and discrimination levels reduced the number of "accidental" coincidences and compensated for systematic imbalances between the two neutron detectors which might lead to false correlation effects.

Several different approaches were made to the problem of identifying "real" correlation features in the data, and reducing the influence of factors which might mask such features. In addition, sets of randomised data were analysed in order to identify correlations in the data which were not attributable to *coincident* neutron constraints.

3.2 PRELIMINARY ANALYSIS

The raw data on buffer tape consisted of:

(a) Multiparameter events in which the following were recorded:

(i) the times-of-flight T_1 and T_2 of *coincident* neutrons (from which the energies E_1 and E_2 would be derived);

(ii) the corresponding recoil proton pulse heights L_1 and L_2 (low-energy thresholds on L_1 and L_2 performed preliminary selection of coincidence events during data acquisition:

an "event" was recorded only if both parameters registered pulse heights above their respective thresholds);

(iii) the "configuration" parameter, which was used in subsequent analysis to identify those events which were recorded at 180°, and at 30° respectively.

(b) Calibration runs for the time-of-flight and pulse height scales, for which the coincidence requirements were relaxed.

These data were first rewritten to another tape on which the word length was compatible with the UNIVAC computer. The blocks containing coincidence data were then extracted and stored on a disk file. Some of these data are presented in figure 3.1 in the raw form in which they were acquired, that is as two-parameter presentations of the times-of-flight T_1 and T_2 of the coincident neutrons.

More accurate estimates of the proton energy threshold of each detector, with its associated PSD system, as well as the neutron detection threshold, were made from density plots of proton pulse height (L) against neutron time-of-flight (T), as described in Chapter 2. The coincidence data were then scanned with windows set on the pulse height and time-of-flight parameters in such a way that the two detectors were subjected to the same cut-offs and recoil proton energy thresholds. It is, however, not possible to achieve identical recoil proton energy cut-off characteristics for the detectors, because each PSD system discriminates against low-energy events in a different manner.

From Run 3, the neutron detection threshold was a relatively high 975 keV, but a much lower threshold of 400 keV was achieved for Run 4.

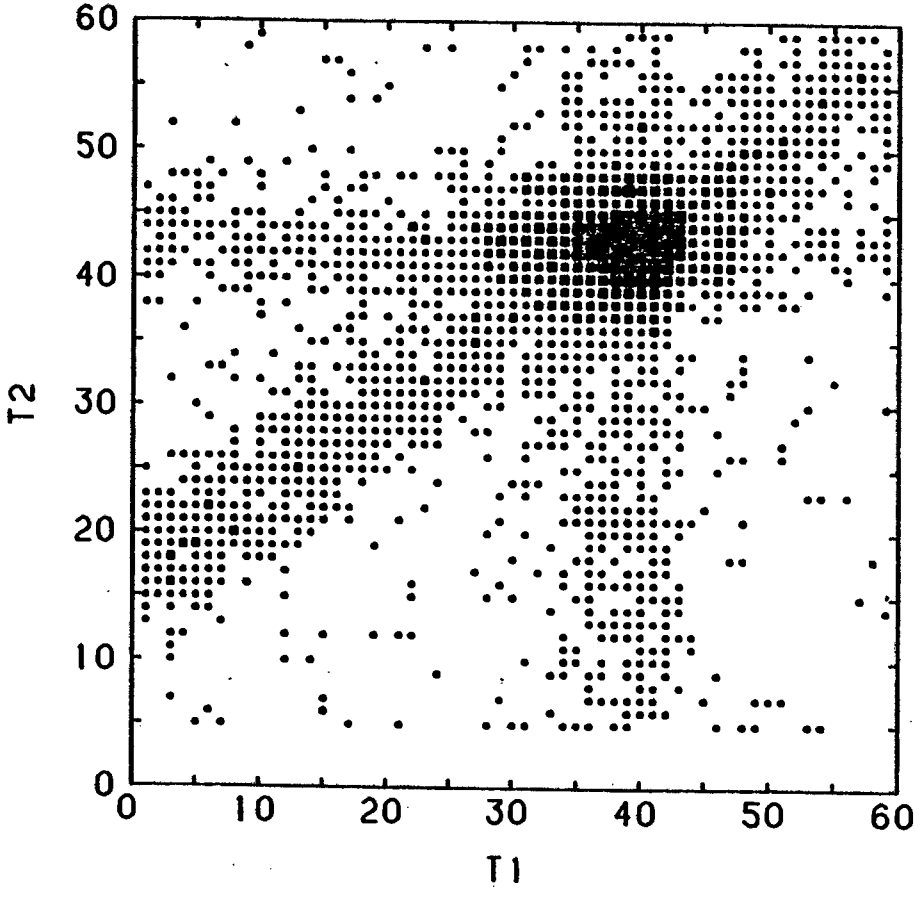

30 DEGREE CONFIGURATION

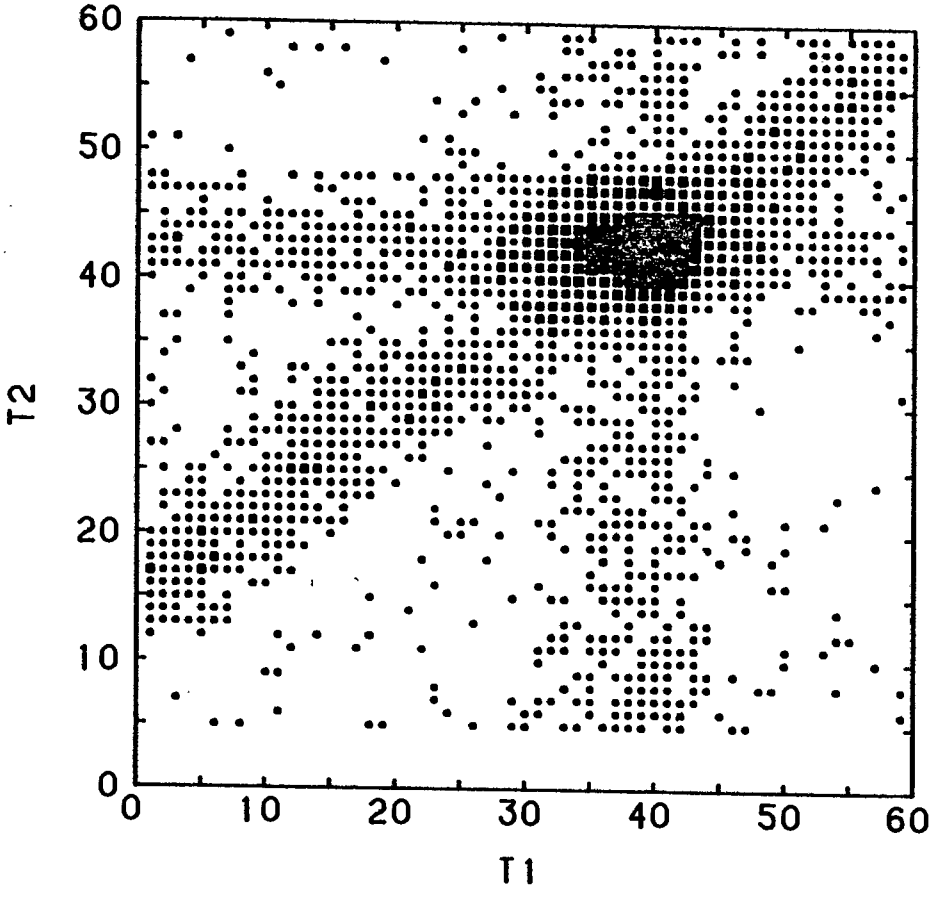

180 DEGREE CONFIGURATION

Figure 3.1: Density plots showing number of events in Run 4 as functions of neutron times-of-flight T_1 and T_2 for coincident neutrons emitted at relative neutron-neutron angles of θ = 30° (left) and 180° (right). The largest squares, which are clustered in the region representing "real" coincidences, each represent >80 counts. The number of counts represented by the other squares, in order of decreasing size is >40, >20, >6 and >1 respectively. The three "bars" of accidental counts, which intersect at the "real" coincidence region are caused by accidental counts in just one of the three detectors. The dispersions of the T_1 and T_2 scales are 3,8 and 5,6 ns per channel respectively.

The total numbers of coincident neutron pairs which survived the selection criteria were:

Run 3: 685 at 30°, and 844 at 180°

Run 4: 3 386 at 30°, and 3 740 at 180°.

277 hours of running time (excluding calibrations, etc.) were necessary to accumulate these 9 000-odd coincident neutron pairs.

Attention was also given to the presence of undesirable accidental counts amongst the true coincidence events. In general, it is not possible to distinguish between accidental and true coincidences falling within the "true" time-of-flight region. Some accidental coincidences betray their identity, however, when the recorded pulse height, that is recoil proton energy, is greater than the neutron "energy" calculated from time-of-flight. These events may be removed from the data by a program which calculates and compares the recoil proton energy (from the calibrated pulse height scales) with the time-of-flight "energy". However, it can be estimated from density plots such as in Figure 3.1 that the proportion of accidental events in the same time-of-flight range as the real events is no more than 4% in Run 3 and 9% in Run 4. The above procedure would remove only some of these accidental events and it was decided that it would be more advisable to leave the data as they were than run the risk of inadvertently introducing spurious asymmetries between the sets of data in the course of removing a few accidental events.

3.3 THE SEARCH FOR CORRELATION EFFECTS

The various methods employed in the attempt to determine whether or not energy-energy correlations were present, and the results from these

methods, are detailed below. During the course of the analysis, it became increasingly apparent that correlation effects, if present at all, were of extremely small magnitude. One or two of the earlier methods employed are thus, with hindsight, not considered sensitive enough to detect these effects, but are nevertheless briefly mentioned. For example, the first method described (Quadrants) was devised as a simple, preliminary test for correlation, before the development of a program to calculate the full Linear Correlation Coefficient.

Method A: Quadrants

The plane defined by E_1 in one dimension and E_2 in the other, where E_1 and E_2 are the energies of the coincident neutrons, is split into quadrants as illustrated in Figure 3.2. Since the quadrants are defined by the medians of the distributions E_1 and E_2,

$$N_1 + N_2 = N_3 + N_4,$$

and $$N_3 + N_2 = N_1 + N_4,$$

from which it is easily determined that $N_1 = N_3$ and $N_2 = N_4$. A comparison between the relative values of N_1 and N_2 is thus sufficient to indicate, in a crude way, whether or not the coincident neutron energies are correlated ($N_1 = N_2$ implies no correlation; $N_1 > N_2$ implies correlation; and $N_1 < N_2$ implies anti-correlation). More concisely, a correlation parameter, ε is defined:

$$\varepsilon \equiv \frac{N_1 - N_2}{N_1 + N_2}$$

The results from only Run 3 are presented here, since this preliminary and approximate method of analysis was superceded by other methods, before

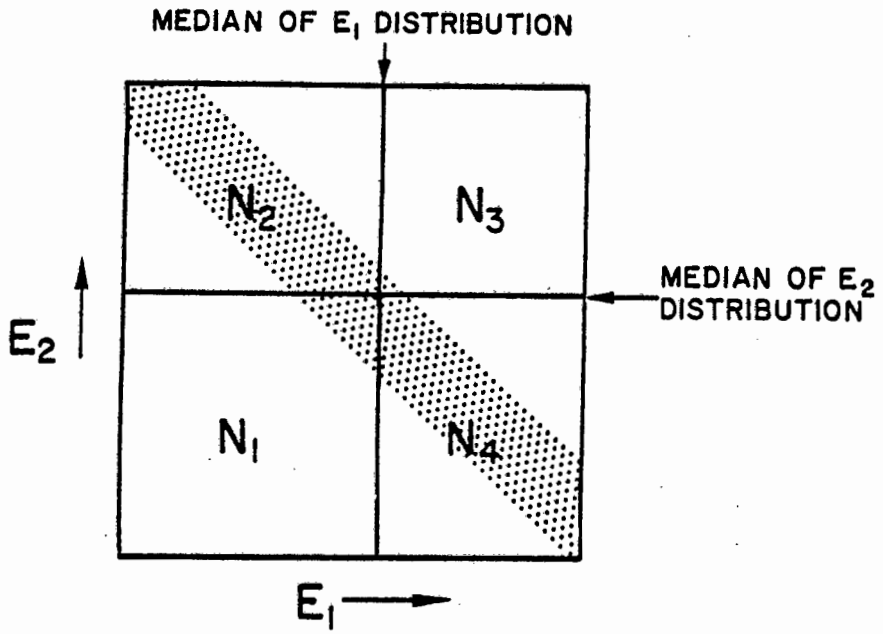

Figure 3.2: Method A (Quadrants). The quadrants are defined by the medians of the distributions E_1 and E_2. The number of coincidence events falling within each quadrant is represented by the values N_1, N_2, N_3, and N_4 respectively. The dotted region represents an hypothetical distribution in which the neutron energies are almost exactly anti-correlated.

the Run 4 data were acquired. The data acquired at each detector configuration were split into three groups in order to check the consistency of the results. The values of ε obtained are presented in Table 3.1.

TABLE 3.1: Values of ε calculated by the Method of Quadrants

	30° configuration	180° configuration
Group 1	0,056	0,064
Group 2	0,010	-0,002
Group 3	0,034	0,063
Mean	0,033	0,041
Standard Deviation of Mean	0,013	0,022

These results do not show any strong correlation trends in the data, although a tendency towards small positive correlations appears in both the 30° and 180° configurations. In order to search for small correlation effects, more sensitive approaches to the analysis were sought.

Method B: Correlation Coefficient

Since the Method of Quadrants is basically a simplified approach to the determination of the linear correlation coefficient, as it is usually defined, the next logical step was to proceed to an exact calculation of this coefficient, with the aim of obtaining more precise results than those of Method A. The linear correlation coefficient is defined by the expression (Pe54):

$$r = \frac{\sum_{i=1}^{N} (E_{1i} - \bar{E}_1)(E_{2i} - \bar{E}_2)}{\left[\sum_{i=1}^{N} (E_{1i} - \bar{E}_1)^2 \sum_{i=1}^{N} (E_{2i} - \bar{E}_2)^2\right]^{\frac{1}{2}}}$$

where N is the total number of coincident neutron energy pairs (E_1, E_2). r can assume values from -1 (exact anti-correlation), through zero (no correlation) to 1 (exact correlation).

Correlation coefficients were calculated for Run 3 and Run 4 (in the case of Run 4, coefficients were also calculated for several subgroups of the data). The results of these calculations are presented in Table 3.2.

TABLE 3.2: Correlation Coefficients

	30° configuration	180° configuration
Run 3, All Events	0,075	0,092
Run 4, All Events	0,120	0,169
Group 1	0,131	0,165
Group 2	0,109	0,168
Group 3	0,082	0,142
Group 4	0,150	0,185
Mean of Groups 1-4	0,118	0,165
Standard Deviation of Mean	0,015	0,009
$\Delta r = r_{180} - r_{30}$	0,047 ± 0,017	

The probability (Pe54) of uncorrelated coincident neutron energies giving rise to the correlation coefficients given in the table is <0,01%. Data from both configurations thus indicate significant correlations. Furthermore, the statistics are good enough (Pe54) to support the conclusion (with 99,5% confidence limits) that the 180° configuration data are more correlated than the data for the 30° configuration.

The correlation coefficients calculated from the Run 3 data might be expected to be different from those determined for the Run 4 data because of the difference between the neutron energy thresholds for the two runs. Although the Run 3 data were not broken up into groups for these calculations, and have therefore not been tested for internal consistency, they do show trends similar to those found in Run 4, namely:

(a) the neutron energies are positively correlated ($r>0$) for both the 30° and 180° configurations; and

(b) the correlation is greater in data acquired in the 180° configuration than in data acquired in the 30° configuration.

In order to test whether the observed correlations were due to some artefact in the data which was not related to coincidence constraints, pairs of *non*-coincident neutron energies were formed from the Run 4 data as follows: for N pairs of coincident neutron energies $(E_{1,x}; E_{2,x})$, $x = 1 \ldots N$, N pairs of non-coincident neutron energies $(E_{1,x}; E_{2,x+1})$ were formed. Correlation coefficients were calculated for three groups of such data, and are given in Table 3.3.

The correlation coefficients for the non-coincident pairs are again significantly different from zero, but smaller in magnitude than those for the coincident pairs.

TABLE 3.3: Correlation coefficients for non-coincident data from Run 4

	30° configuration	180° configuration
Group 1	-0,024	0,020
Group 2	-0,025	0,012
Group 3	-0,022	0,005
Mean coefficient	-0,024	0,012
Standard Deviation of Mean	0,001	0,004
$\Delta r = r_{180} - r_{30}$	0,036 ± 0,004	

The coefficients calculated for the coincident and non-coincident pairs respectively, are summarised for comparison in Table 3.4.

TABLE 3.4: Comparisons between the correlation coefficients calculated for coincident energy pairs and those calculated for non-coincident energy pairs

	r_{30}	r_{180}	$\Delta r = r_{180} - r_{30}$
Coincident pairs	0,118±0,015	0,165±0,009	0,047±0,017
Non-coincident pairs	-0,024±0,001	0,012±0,004	0,036±0,004
(Coinc.) - (Non-coinc.)	0,142±0,015	0,153±0,010	0,011±0,017

These results suggest that

(a) the higher correlation coefficients found for the coincident pairs may be attributable to energy correlations between neutrons from the same *fission*.

(b) since the differences Δr between the 180° and 30° coefficients are similar for the coincident and non-coincident pairs (Δr = 0,047 and 0,036 respectively), they may be caused by differences in the *geometry* between the 180° and 30° configurations, rather than in the physics of coincident neutron emission.

Method C: $E_1 + E_2$

A comparison was made between the 30° configuration data and the 180° configuration data as follows: Energy distributions (normalised to the same integral) were obtained by summing the two coincident neutron energies. A marked correlation effect in one set of data which was not present in the other would result in a noticeable difference between the shapes of these distributions, as can be seen from the schematic diagram, Figure 3.3.

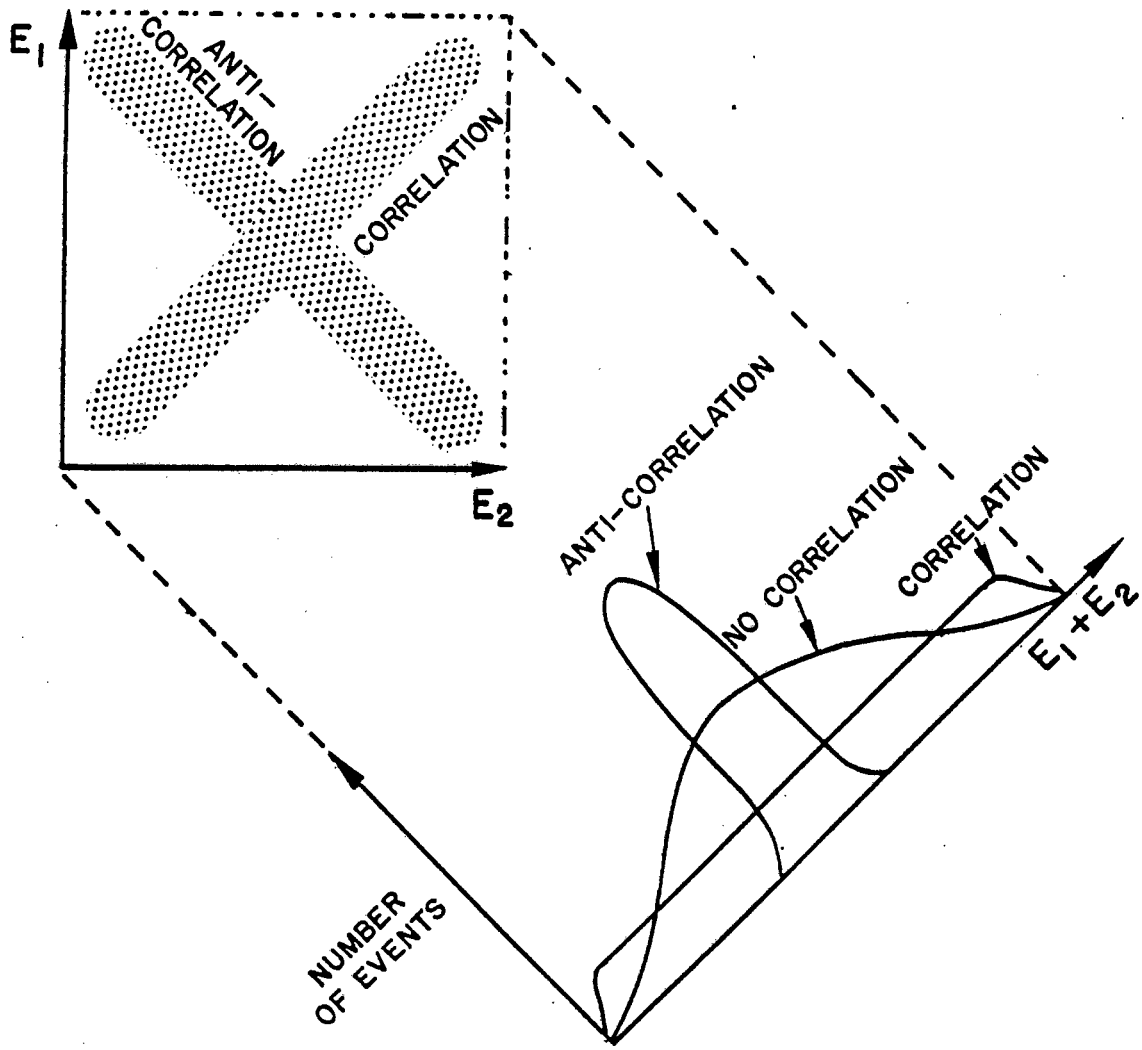

Figure 3.3: Schematic illustration of how the distribution of the sums of coincident neutron energies, $E_1 + E_2$, is sensitive to correlation effects. For ease of illustration here uniform (rather than Maxwellian) energy distributions are assumed for E_1 and E_2. Strongly correlated data would then be clustered into a narrow band on the $(E_1; E_2)$ plane and the projection of this band would be a uniform distribution on the $E_1 + E_2$ axis. In contrast, strongly anti-correlated data would result in a sharply peaked distribution of $E_1 + E_2$.

If one set of data were, for instance, more strongly anti-correlated than the other, the distribution of $E_1 + E_2$ for the former would be enhanced at average energies and deficient at low and high energies with respect to the latter. The comparisons are shown in Figure 3.4 (Run 3) and Figure 3.5 (Run 4).

Statistical scatter makes a critical comparison of the two histograms in each figure very difficult. It is easier to assess the differences between them when one is subtracted from the other and only the residual distribution is plotted, which is illustrated in Figures 3.6 (Run 3) and 3.7 (Run 4).

It appears that, for this method of comparison, inadequate statistical accuracy is the limiting factor. The next method of analysis described is an attempt to overcome this problem.

Method D: Integral Distributions

This method was a small variation on Method C. If N represents "number of events" and $E = E_1 + E_2$, that is the sum of the two coincident neutron energies, then distributions were formed of $N_{>E}$ versus E. The advantage of these "reversed" integral distributions over those formed by Method C is that they are smoother (i.e. affected less by statistical fluctuations). Even a relatively small difference in shape between the distributions formed from the 30° and 180° data respectively, would thus be apparent. Plots of these distributions are given in Figures 3.8 and 3.9 for Runs 3 and 4 respectively.

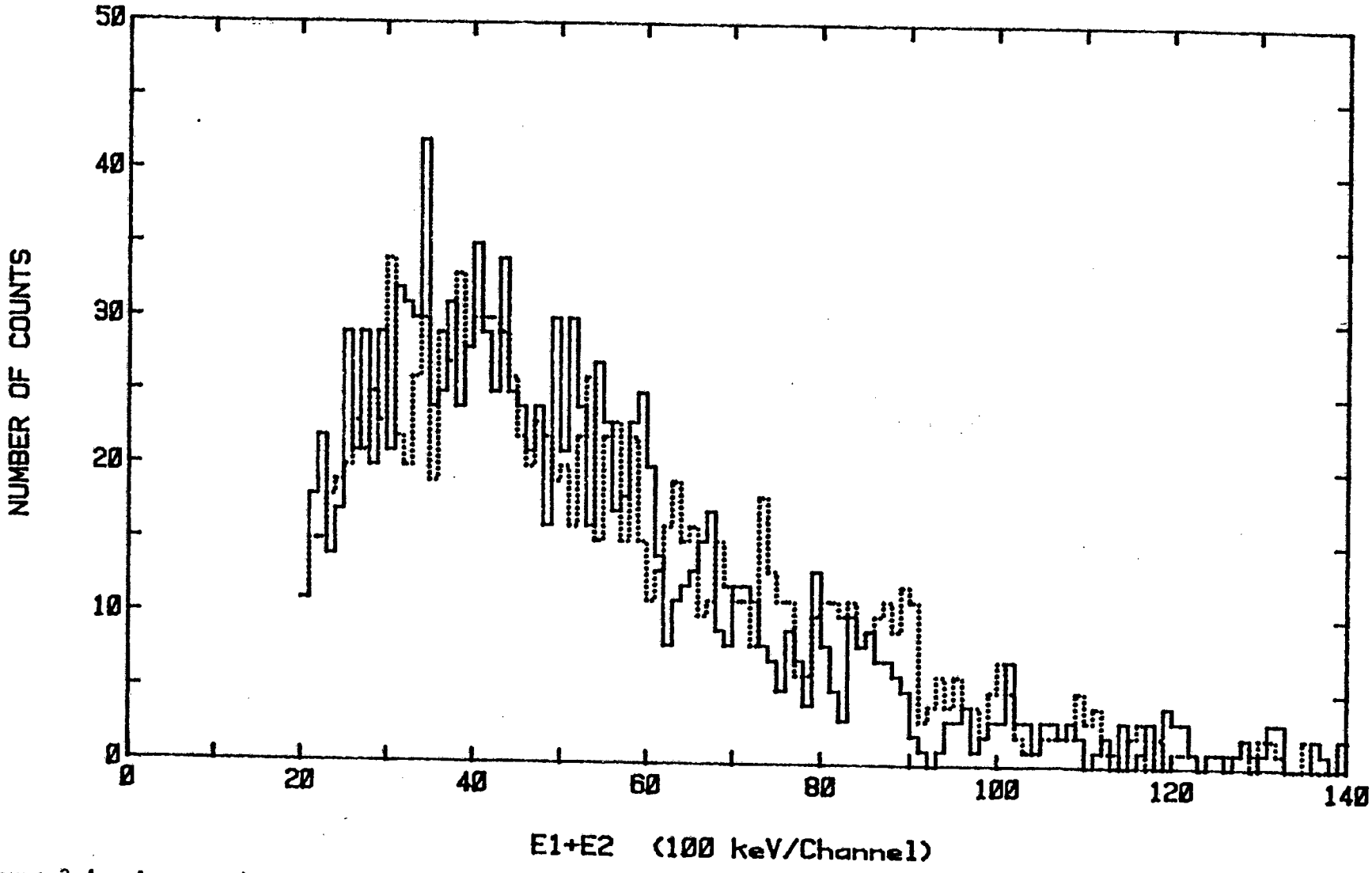

Figure 3.4: A comparison between the distributions of the sum of coincident neutron energies, $E_1 + E_2$, measured at 30° (solid line) and 180° (dotted line) for the data from Run 3. The distributions are normalised to represent the same number of counts, with an energy threshold of 975 keV for individual neutrons, which gives rise to a threshold of 1,95 MeV for $E_1 + E_2$.

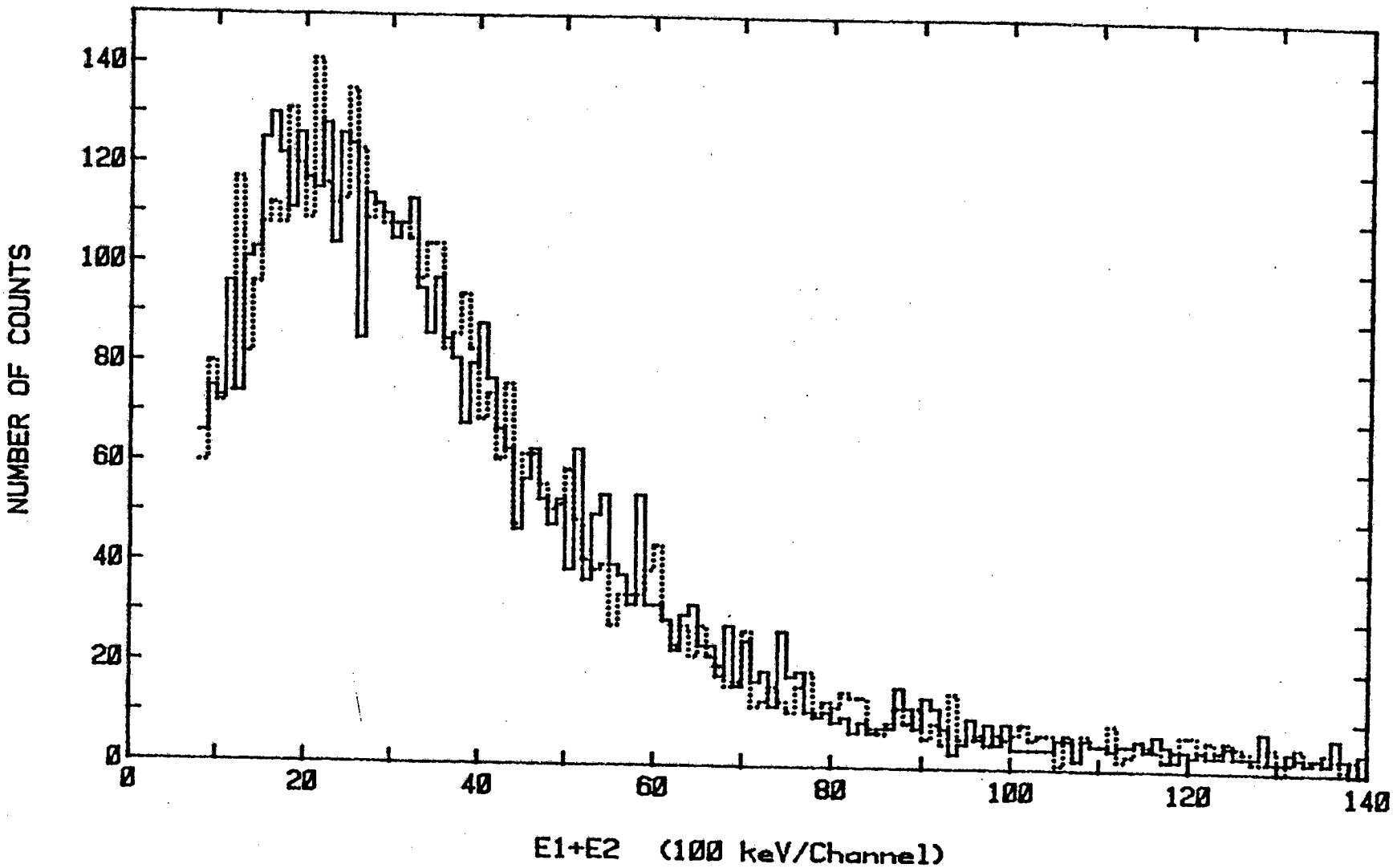

Figure 3.5: A comparison between the distributions of the sum of coincident neutron energies, $E_1 + E_2$, measured at 30° (solid line) and at 180° (dotted line) for the data from Run 4. The distributions are normalised to represent the same number of counts, with an energy threshold of 400 keV for individual neutrons, which gives rise to a threshold of 800 keV for $E_1 + E_2$.

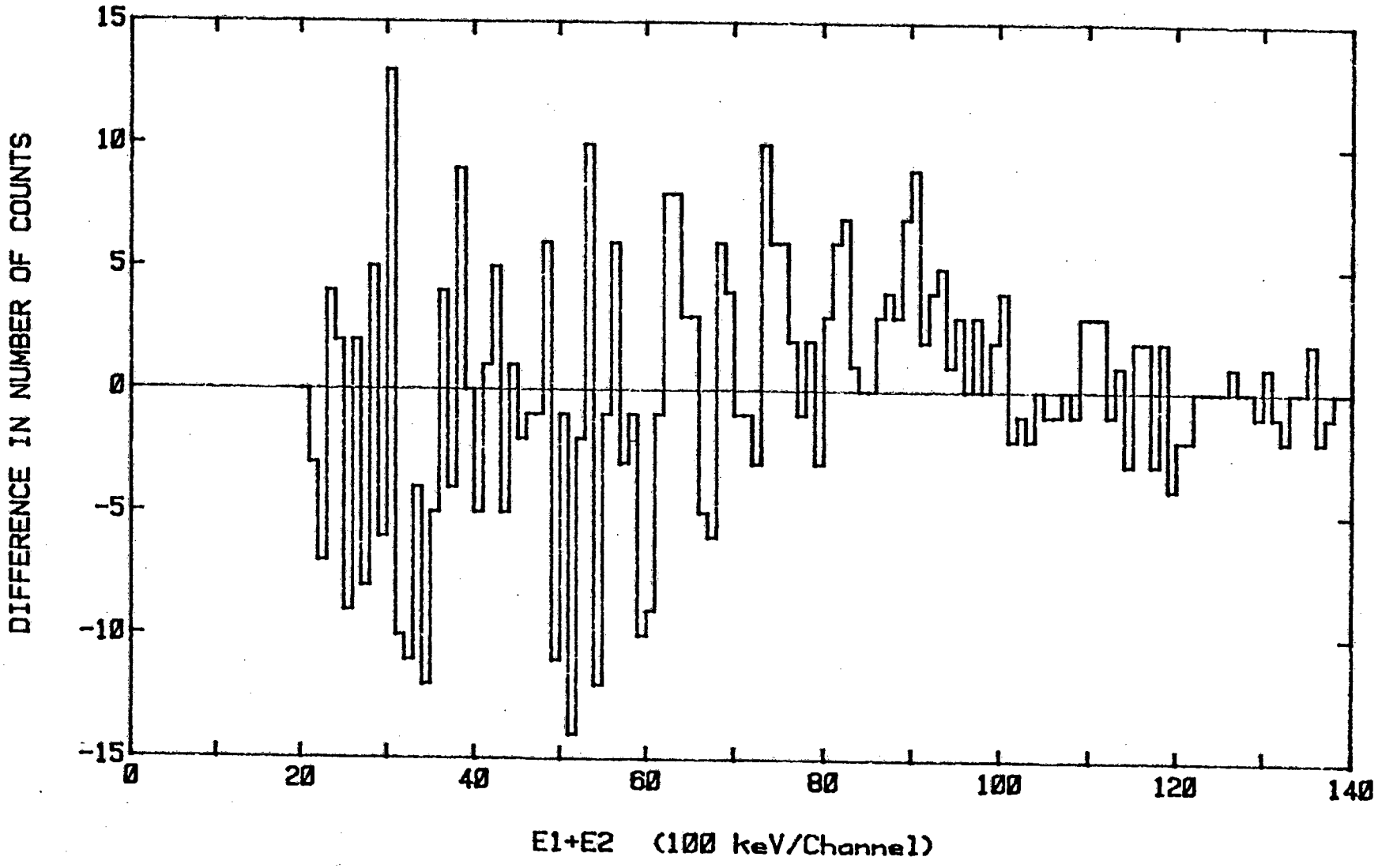

Figure 3.6: Difference between the dotted line (180° configuration) and the solid line (30° configuration) of Figure 3.4, Run 3

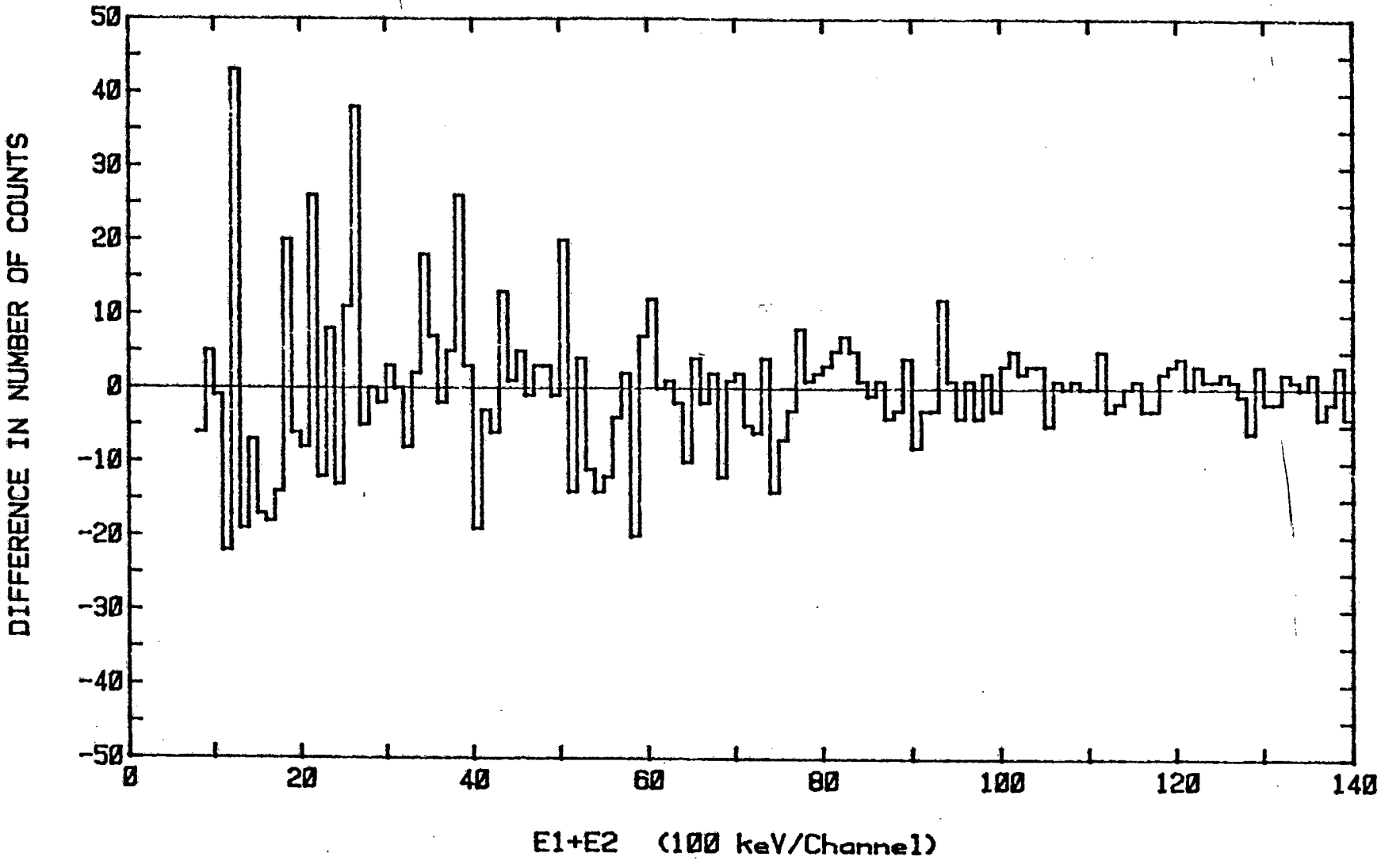

Figure 3.7: Difference between the dotted line (180° configuration) and the solid line (30° configuration) of Figure 3.5, Run 4.

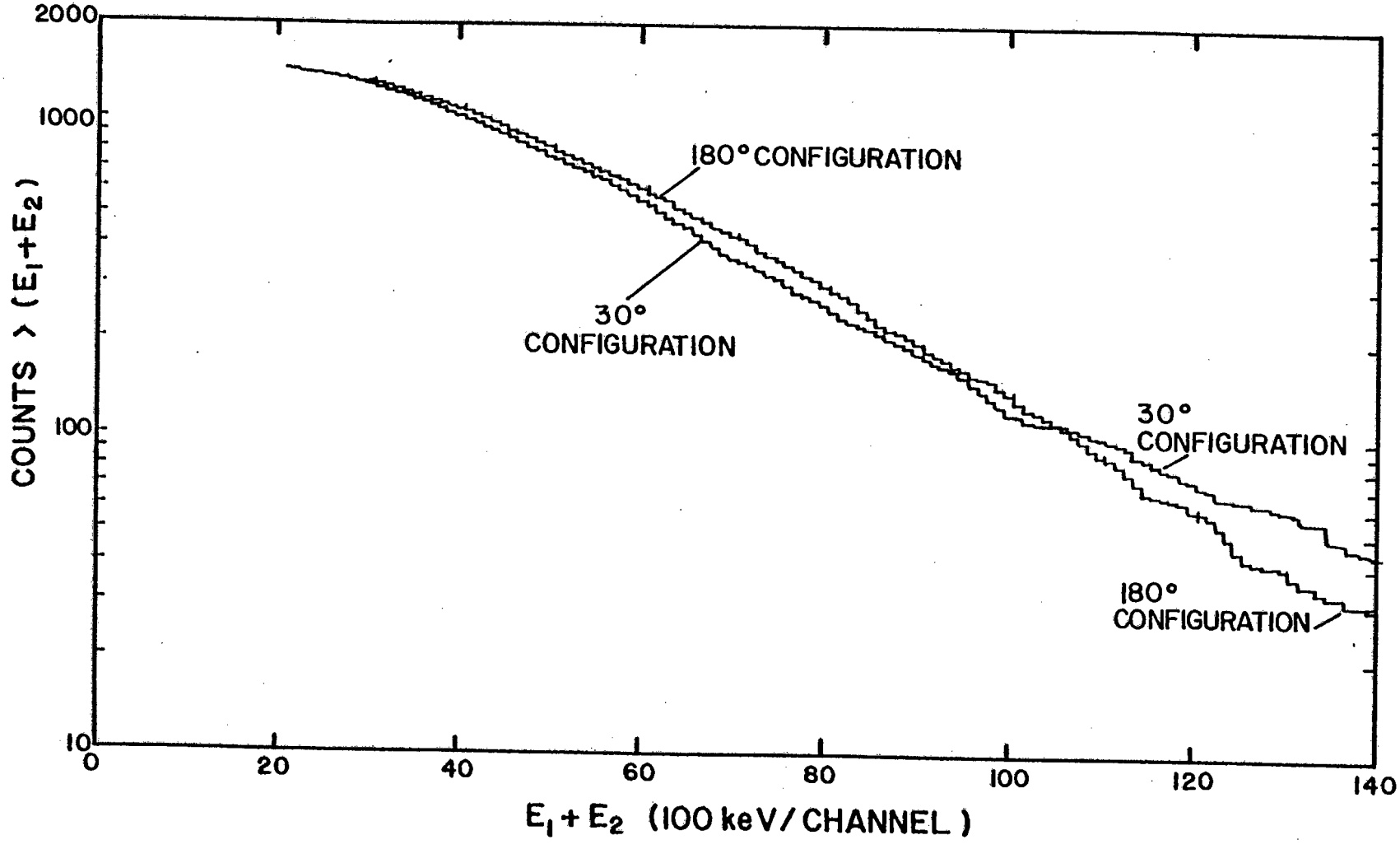

Figure 3.8: Results from Method D: Integral Distributions, for Run 3. The number of events greater than $E_1 + E_2$ is plotted against $E_1 + E_2$. The curves are normalised to represent the same number of total counts.

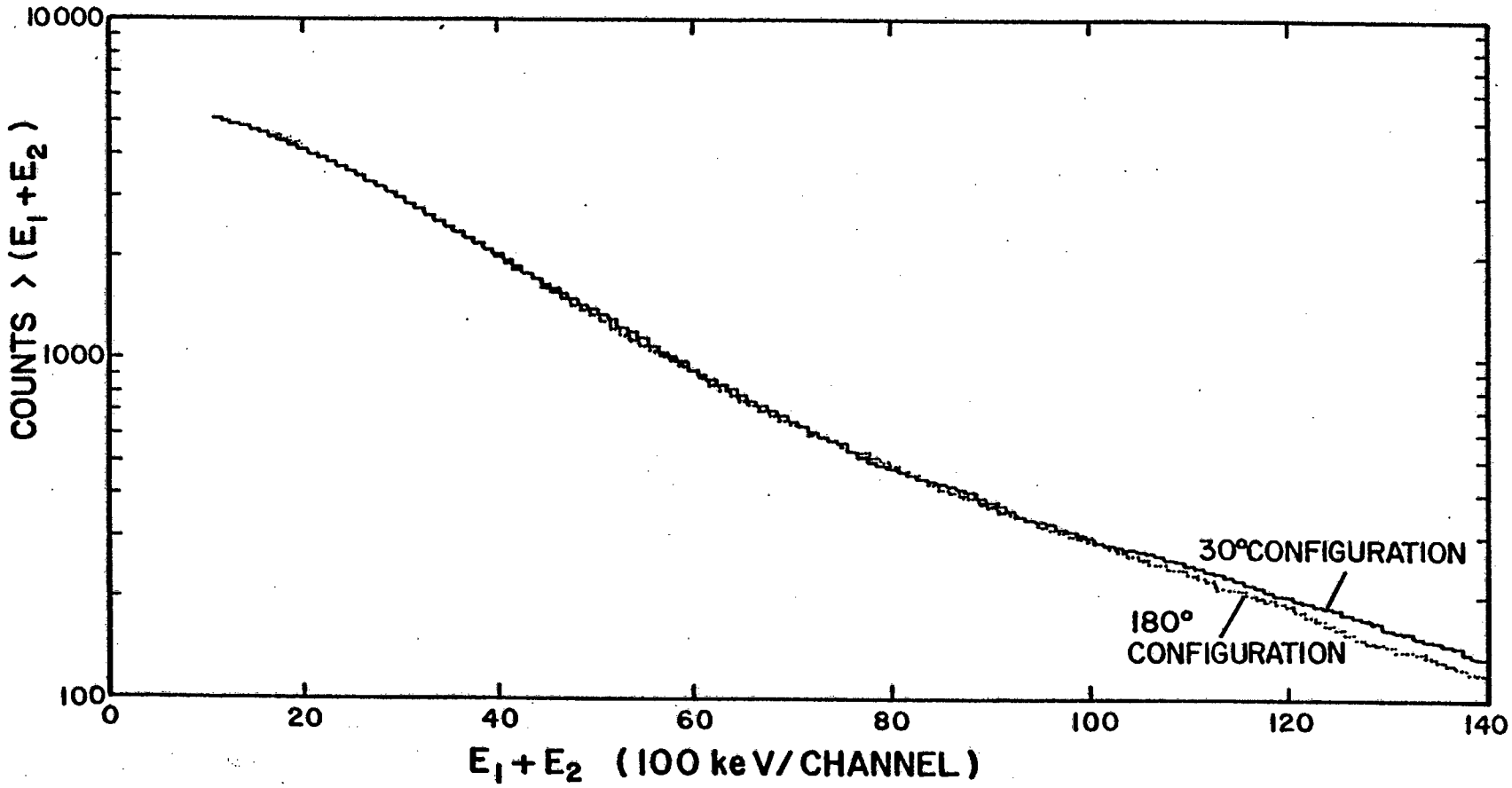

Figure 3.9: Results from Method D: Integral Distributions, for Run 4. The number of events greater than $E_1 + E_2$ is plotted against $E_1 + E_2$. The curves are normalised to represent the same number of total counts.

Both for Run 3 and Run 4, the distribution for the 30° configuration falls off more slowly at high energies than the distribution for the 180° configuration, which implies that there are relatively more events at total energies exceeding 14 MeV at the 30° configuration (although the figures extend only to 14 MeV, the high-energy cutoff used for these calculations was 20 MeV). However, it should be noted that the figures are plotted on a logarithmic scale in the vertical axis; the intensities of the Maxwellian spectra at such high energies are so low that the differences observed are not statistically significant.

Method E: Ratio

None of the above methods takes account of the spread in the initial excitation energy of the fission fragments. Bowman *et al.* (Bo 63) calculated, from their measurements, the average excitation energy appearing in the form of prompt neutrons, as a function of fragment mass (see Figure 3.10). This distribution, which should be expected to resemble very closely the distribution of total excitation energies, exhibits a strong saw-tooth dependance on fragment mass, with excitation energies ranging from less than 10 MeV to more than 30 MeV. At first glance, the implications of this extremely large variation in initial excitation energies would seem to be that any search for correlation effects in the energies of prompt neutrons could not succeed unless the initial excitation energy were somehow measured or calculated. Fortunately, however, the problem is not nearly as serious as it might appear, if one considers the distribution of the mass yield of fission fragments (Wh63, Sc66, Ga74, Wa77, Ki82). The distribution has a "double-humped" shape (see Figure 3.11): ∿70% of ^{252}Cf fissions give rise to fragments in the mass range 102 - 117 a.m.u. (light fragment)

an "event" was recorded only if both parameters registered pulse heights above their respective thresholds);

(iii) the "configuration" parameter, which was used in subsequent analysis to identify those events which were recorded at 180°, and at 30° respectively.

(b) Calibration runs for the time-of-flight and pulse height scales, for which the coincidence requirements were relaxed.

These data were first rewritten to another tape on which the word length was compatible with the UNIVAC computer. The blocks containing coincidence data were then extracted and stored on a disk file. Some of these data are presented in figure 3.1 in the raw form in which they were acquired, that is as two-parameter presentations of the times-of-flight T_1 and T_2 of the coincident neutrons.

More accurate estimates of the proton energy threshold of each detector, with its associated PSD system, as well as the neutron detection threshold, were made from density plots of proton pulse height (L) against neutron time-of-flight (T), as described in Chapter 2. The coincidence data were then scanned with windows set on the pulse height and time-of-flight parameters in such a way that the two detectors were subjected to the same cut-offs and recoil proton energy thresholds. It is, however, not possible to achieve identical recoil proton energy cut-off characteristics for the detectors, because each PSD system discriminates against low-energy events in a different manner.

From Run 3, the neutron detection threshold was a relatively high 975 keV, but a much lower threshold of 400 keV was achieved for Run 4.

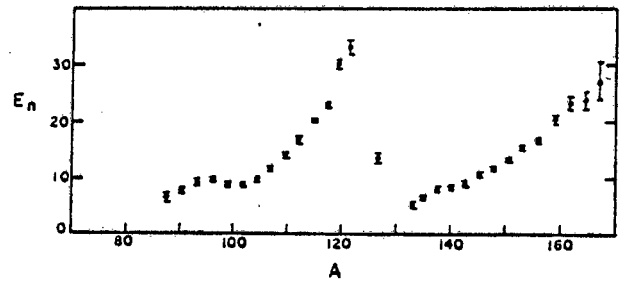

Figure 3.10: The average excitation energy E_n, appearing in the form of prompt neutrons, as a function of mass. (Figure from Bo63).

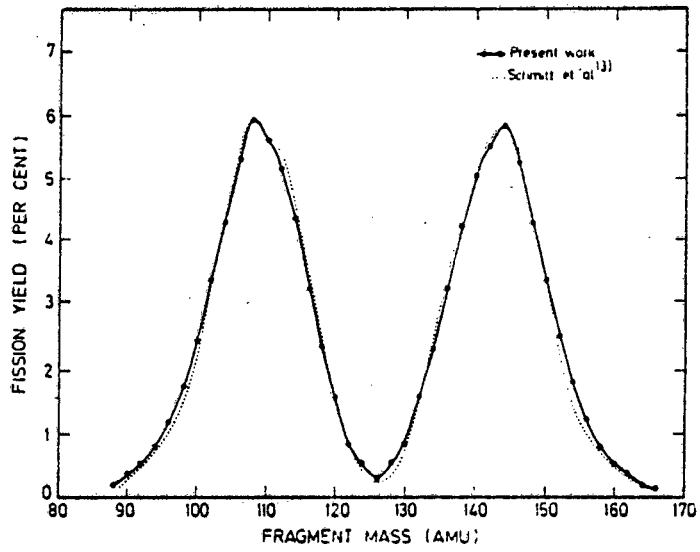

Figure 3.11: Mass yield curve for ^{252}Cf, the results of Walsh and Boldeman (solid line, Wa77) and of Schmitt *et al.* (dotted line, Sc66). (Figure from Wa77).

and 136 - 151 a.m.u. (corresponding heavy fragment). With reference to Figure 3.10, it is thus apparent that middle-of-the-range values for initial excitation energy are predominant.

Nevertheless, the possibility cannot be discounted that small correlation effects may not be detectable by any method of analysis which fails to take into account the differences in initial excitation energy from one fragment to the next. Consequently, the energy measurements were analysed in terms of the frequency distribution of the ratio $R = E_{Lo}/(E_{Lo} + E_{Hi})$, where E_{Lo} and E_{Hi} are the lower and higher energies respectively for a coincident neutron pair. Since ~80% of the Initital Excitation Energy of a fragment appears in the form of prompt neutrons (Bo78, Sk80, Sp82), and the binding energy per neutron is more or less constant at ~5 MeV (Bo63), the sum of the coincident neutron energies, $E_{Lo} + E_{Hi}$, is roughly proportional to the Initial Excitation Energy for cases in which the neutrons are emitted from the same fragment, and thus serves as a normalising factor with respect to different Initial Excitation Energies (except, of course, for ~20% of the fragments which emit more than two neutrons (Sc66, Si72, Wa77)). Where the neutrons originate from opposite fragments, this is not necessarily always the case, as will be discussed in Chapter 4, but in general, the frequency distribution of R is less sensitive to variations in Initial Excitation Energy than is the straight-forward distribution of neutron energies.

The computer program which was written to form the frequency distributions, R, used a random number generator to eliminate "integer" effects, such as the predominance of exact fractions (1/2, 1/3, 2/3, etc.),

caused by the data having been recorded in digital form. For instance, any neutron assigned to energy "bin" x, was allocated a "real" energy in the range between the energies represented by "bin" x and "bin" (x+1).

Figure 3.12 is a sketch of some hypothetical R-distributions under different correlation constraints.

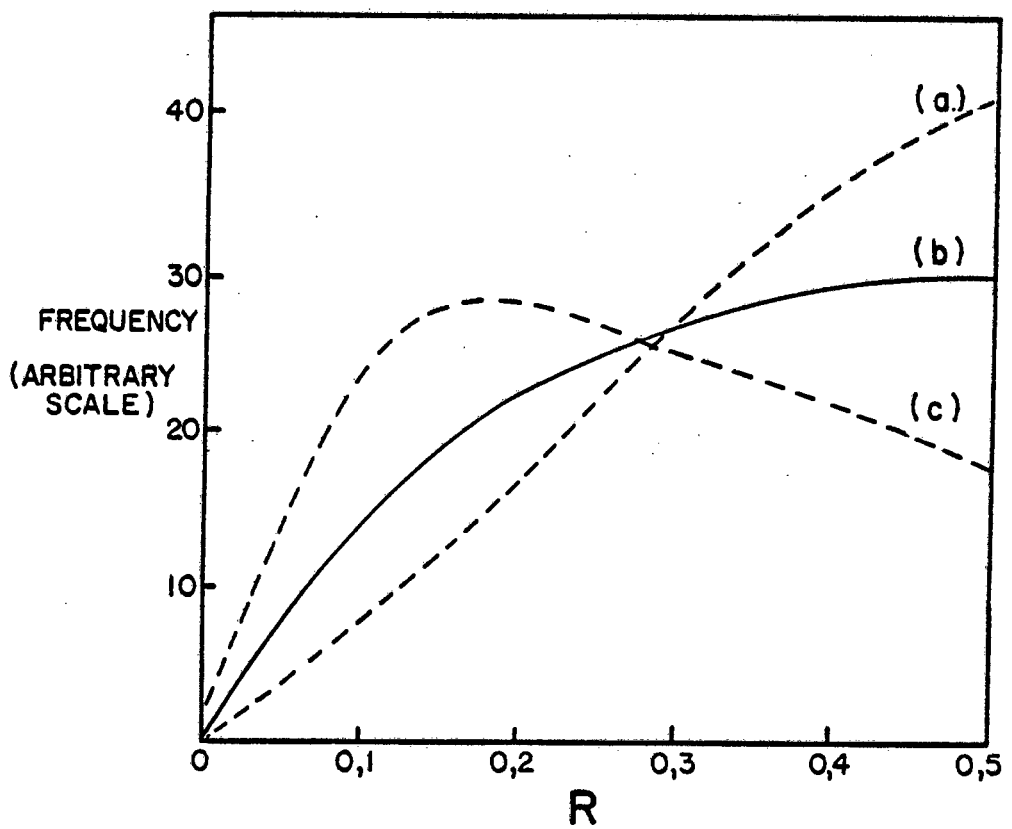

Figure 3.12: Expected shape of R-distributions if:
(a) E_1 and E_2 are strongly correlated;
(b) E_1 and E_2 are uncorrelated;
(c) E_1 and E_2 are strongly anti-correlated.

In order to check for any systematic experimental asymmetries between the 30° and 180° geometries, the ratio R' was also calculated in which each neutron was paired successively with the *non*-coincidental neutrons in the data set for the same geometry. Since a very large number of such combinations exists, the distribution of the random ratios, R', were determined with greater statistical accuracy than those of the true ratios, R.

The results of these calculations of R and R' are presented in Figures 3.13 and 3.14 respectively.

In order to facilitate the comparison, the residual distributions (30° distributions subtracted from 180° distributions) are given in Figure 3.15, for both R (histogram) and R' (curve).

There does not appear to be a systematic difference between the R-distributions from coincident neutron energies measured at 30° and 180° respectively. The "dip" in the residual distribution for Run 3 (Figure 3.15(a)) near R = 0,5 is not present in the distribution for Run 4. Similarly, the "dip" in the Run 4 residual distribution around R = 0,1 is not repeated in the Run 3 distribution. In any case, even the largest residuals in these regions are within two standard deviations from zero, so that random statistical fluctuations could well be responsible for them.

The differences between the R'-distributions (non-coincidental neutrons) formed from the 30° and 180° data respectively are undoubtably systematic, however, if one considers the large number of energy pairs which were drawn from the data, and the consistency of the trend in the

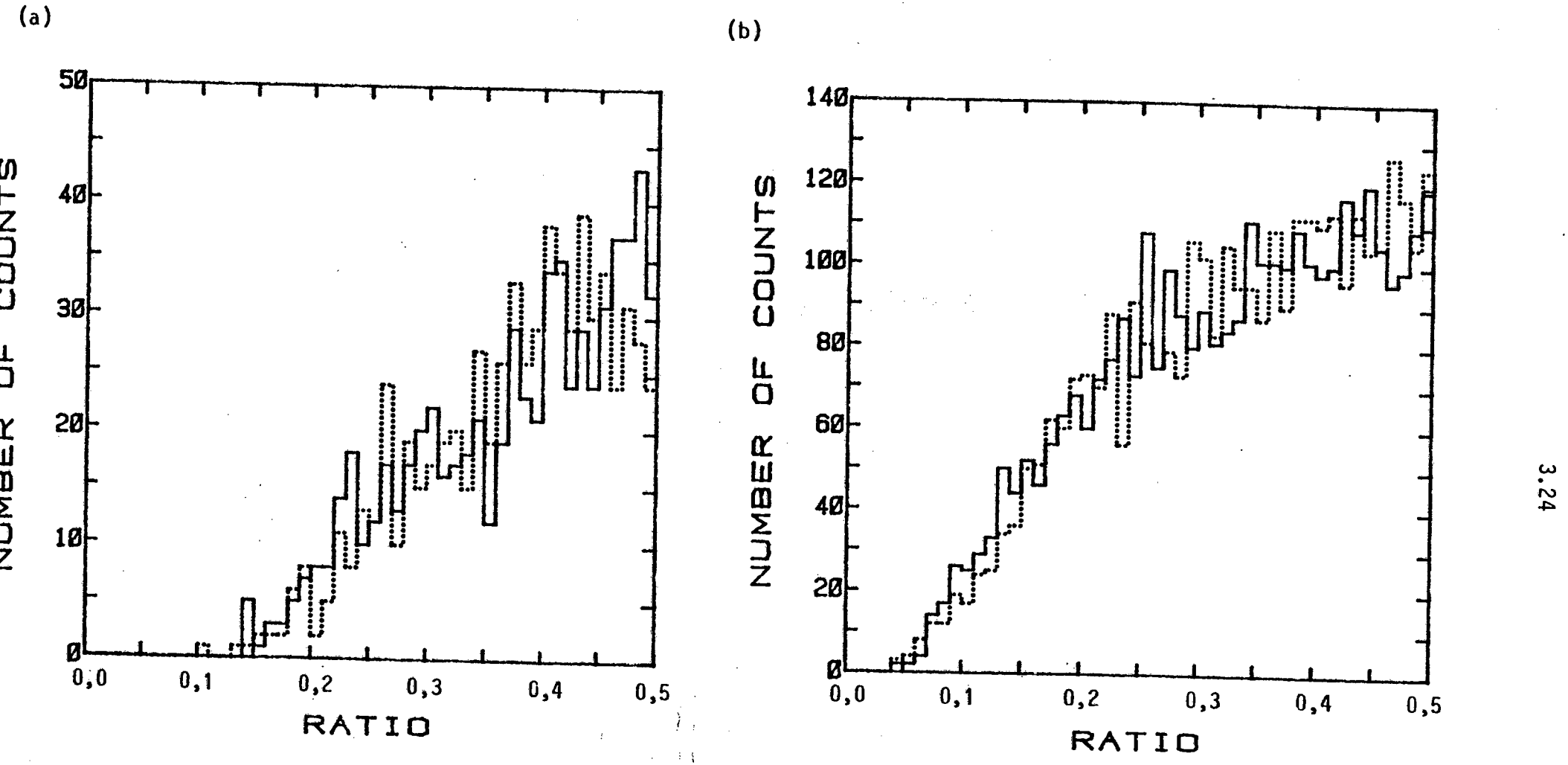

Figure 3.13: Comparisons between the frequency distributions of the ratio $R = E_{Lo}/(E_{Lo} + E_{Hi})$, calculated from data measured at 30° (solid line) and at 180° (dotted line). The distributions are normalised to represent the same number of counts. Results from Run 3 and Run 4 are shown in (a) and (b) respectively.

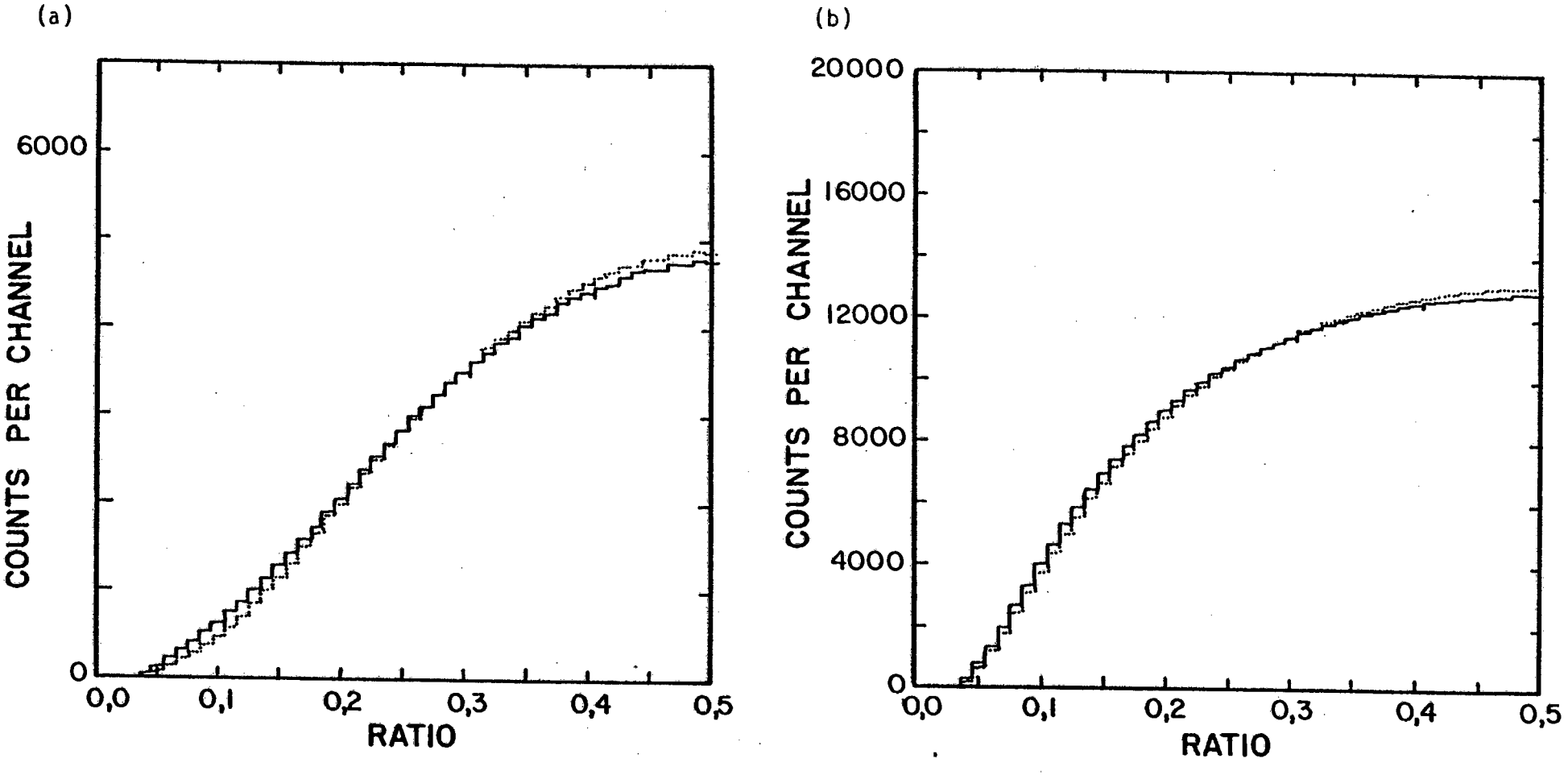

Figure 3.14: Comparisons between the frequency distributions of the ratio $R' = E_{Lo}/(E_{Lo} + E_{Hi})$, where the E_{Lo} and E_{Hi} are the energies of *non*-coincidental neutrons drawn from the data set for the same geometry. The calculated distributions from data measured at 30° (solid lines) and at 180° (dotted lines) are normalised to represent the same number of counts. Results from Run 3 and Run 4 are shown in (a) and (b) respectively.

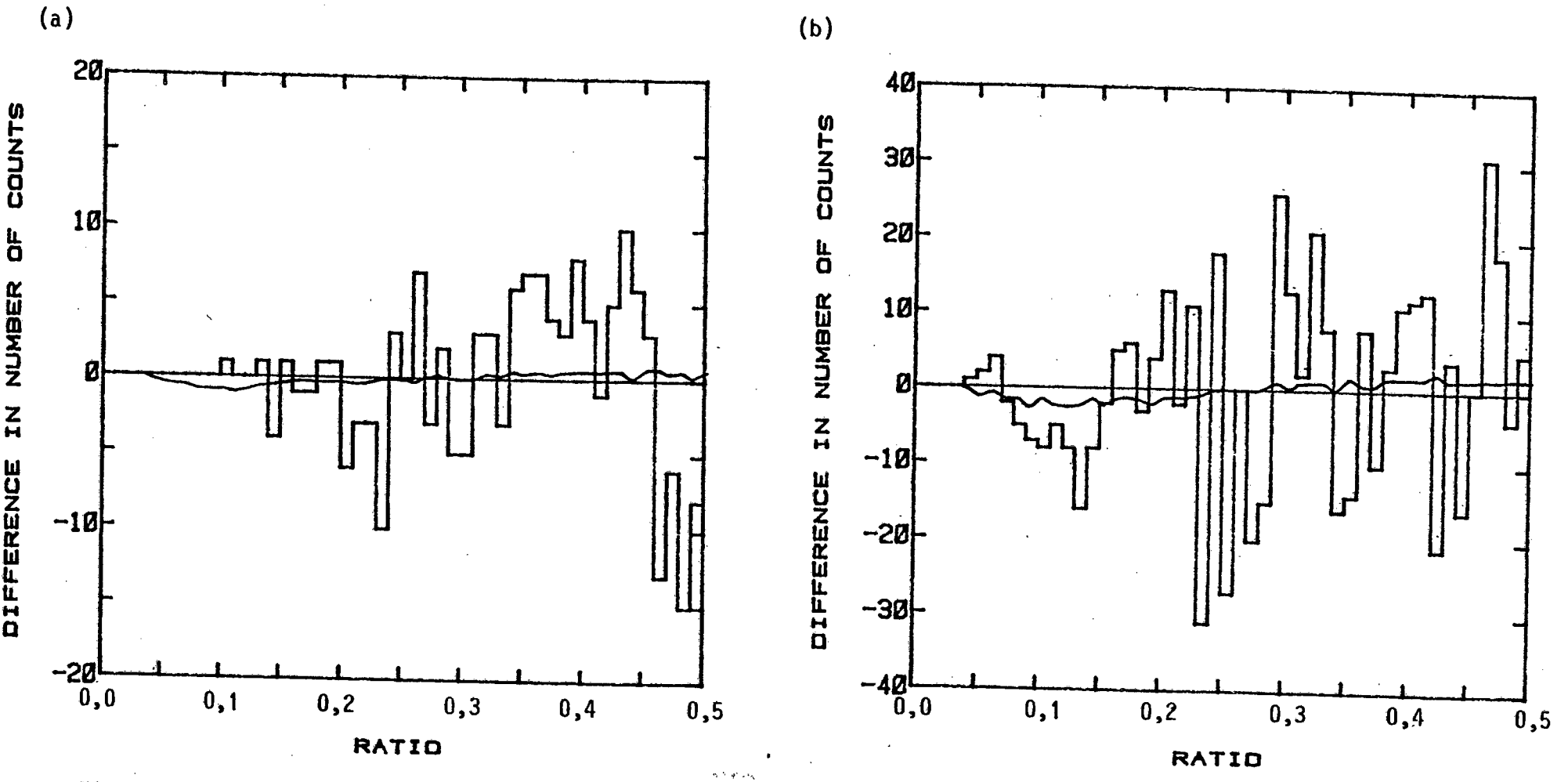

Figure 3.15: Residual Distributions: the histograms represent the difference between the dotted line (180° configuration) and the solid line (30° configuration) of Figure 3.13 (R-distributions) for (a) Run 3, and (b) Run 4. The curves represent the corresponding differences in the R'-distributions of Figure 3.14, normalised to the same total number of events as are presented in the R-distributions.

independent data from Runs 3 and 4. The 180° distributions are enhanced near R = 0,5 with respect to the 30° distributions, which implies that the single-neutron energy spectra are less dispersed in the data from 180° measurements than are those from 30° measurements. It should be noted that these spectra are not the same as the true "singles" spectra, since they were acquired under coincident neutron constraints.

Method F: Medians of R-distributions

Enhancement of the R-distribution for the 30° configuration at low values of R with respect to the distribution for the 180° configuration would be evidence of an anti-correlation effect at that angle; conversely, enhancement near R = 0,5 would point to a correlation of neutron energies. A simple way of checking this is to compare the positions of the medians of the distributions. These are shown in Figure 3.16.

The values calculated, with their respective standard deviations are as follows: (the expression of the medians and their errors in terms of fractions of integral Channel Numbers is a somewhat dubious exercise, but it serves at least to give some idea of the relative magnitudes of these quantities)

	30° configuration	*180° configuration*
Run 3	Channel 39,1±0,8	Channel 39,0±0,6
Run 4	Channel 34,0±0,4	Channel 34,3±0,4

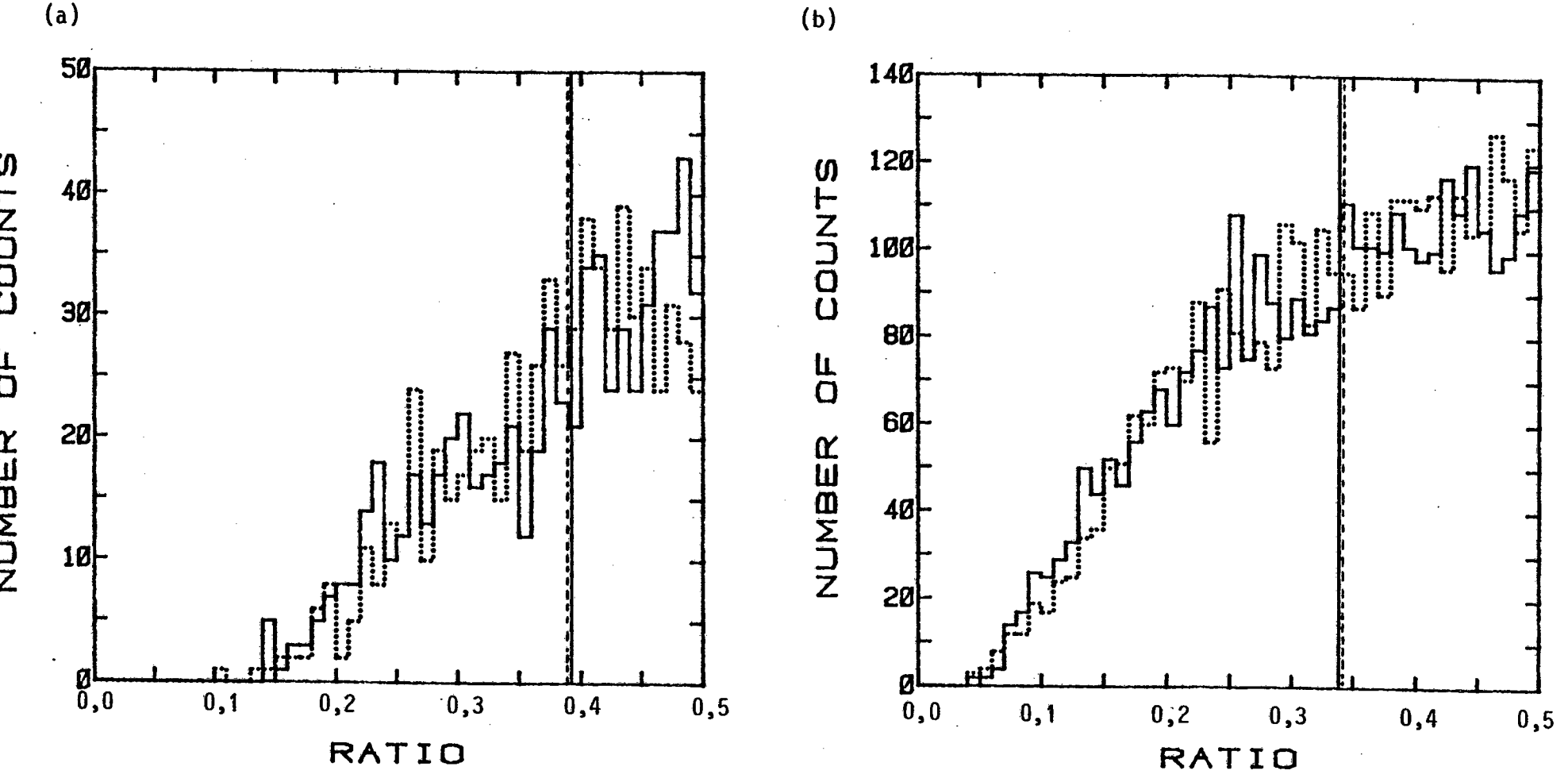

Figure 3.16: The positions of the medians of the R-distributions from Figure 3.13 are represented by the solid lines (30° configuration) and the dotted lines (180° configuration).

It is obvious from these results that this method is insensitive to small systematic differences between the distributions, if they exist at all.

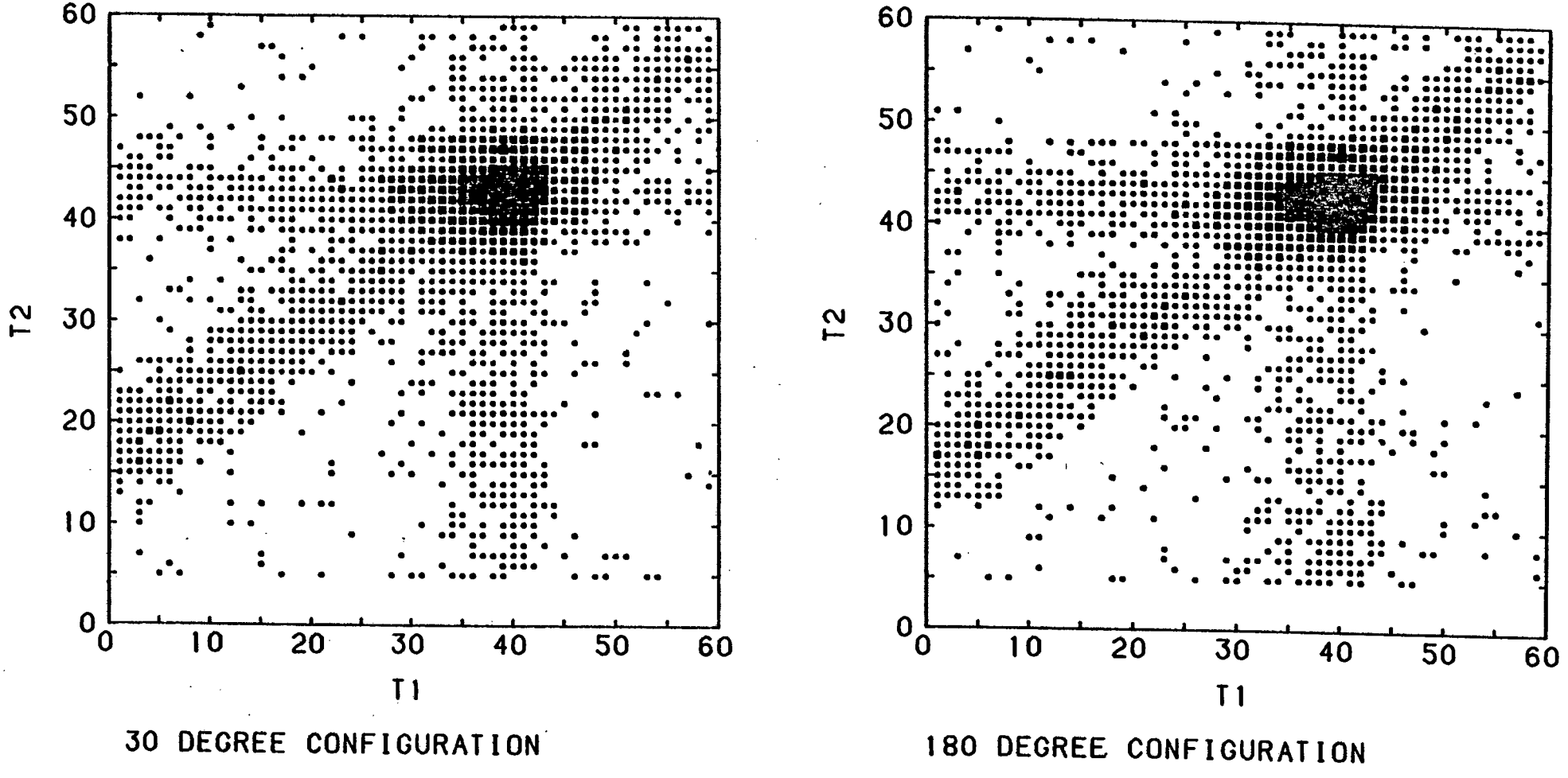

Figure 3.1: Density plots showing number of events in Run 4 as functions of neutron times-of-flight T_1 and T_2 for coincident neutrons emitted at relative neutron-neutron angles of $\theta = 30°$ (left) and 180° (right). The largest squares, which are clustered in the region representing "real" coincidences, each represent >80 counts. The number of counts represented by the other squares, in order of decreasing size is >40, >20, >6 and >1 respectively. The three "bars" of accidental counts, which intersect at the "real" coincidence region are caused by accidental counts in just one of the three detectors. The dispersions of the T_1 and T_2 scales are 3,8 and 5,6 ns per channel respectively.

CHAPTER 4

DISCUSSION

4.1 SUMMARY OF RESULTS

The results from the calculation of the linear correlation coefficient (Method B) indicate that there is a correlation of coincident neutron energies, and that the correlation is more pronounced at 180° than at 30° (see Table 3.2). Results from the less sensitive Method of Quadrants (see Table 3.1) broadly support these findings.

None of the Methods C ($E_1 + E_2$), D (Integral Distributions), E (Ratio) and F (Medians of Ratio) contribute any further information about correlations of coincident neutron energies, presumably due to inherent lack of sensitivity of the methods themselves.

It was hoped that the method, Ratio, being the only one which made any allowance for the variances in initial excitation energies of the fragments, would allow a more critical test for the presence of correlations (see Figures 3.13 and 3.14). The interpretation of any results from this method should, in any case, be approached with caution. If, for instance, the variation in initial excitation energy affects the *average* neutron energy from one fragment to the next to a greater extent than the cascade cooling phenomenon affects the energies of neutrons from a particular fragment, the distribution of $E_{Lo}/(E_{Lo} + E_{Hi})$ would probably be less correlated when the coincident neutrons originate from opposite fragments (at 180°) than when they are emitted in a cascade from the same fragment (at 30°). To some

extent, therefore, the method is self-defeating, for the larger the influence of the effect for which it attempts to compensate (variation in initial excitation energy), the more uncertainty is cast upon the comparison of the two distributions of R as a valid test for correlation features in one distribution which are not present in the other. It is thus possible that failure to detect an appreciable difference between the distributions for neutrons from the same fragment and from opposite fragments respectively is a manifestation of an anti-correlation effect on each, of separate origin but comparable magnitude.

4.2 ASYMMETRIES ASSOCIATED WITH THE GEOMETRIES

If there are no systematic asymmetries associated with the different geometries in the recording of data in either configuration, then the single-neutron energy distribution measured by each detector should be independent of whether the mobile detector is in the 30° or 180° position. Thus, if instead of coincident neutron energy pairs, distributions of *non*-coincidental energy pairs are formed, such distributions formed from the energy measurements at 30° should be indistinguishable from those formed from the measurements at 180°.

This hypothesis was tested by two of the methods described in Chapter 3. The correlation coefficients calculated for groups of non-coincidental neutron pairs (see Table 3.3) indicate that there is indeed a difference: the pairs formed from the 180° data are more correlated than those formed from the 30° data.

For the method, Ratio, each neutron was paired successively with *every other* non-coincidental neutron in the data set for the same geometry, which ensured good statistical accuracy of the results. A comparison between the distributions of R' (see Figure 3.15) confirms the earlier result that there is more correlation present in the 180° neutron data than in the 30° neutron data.

There are various possible explanations for these results: changes in the time-of-flight distance, electronic drifts, cross-talk between the liquid scintillators, accidental coincidences and asymmetries associated with differences in neutron multiplicity. Each is treated in turn below.

Time-of-flight distance, D: The mobile detector was firmly clamped to a rod which pivoted about a point directly beneath the ^{252}Cf source (see Figures 2.2 and 2.3). The source-to-detector distance was checked several times at both detector positions and found to be constant, so it is unlikely that any differences in the distance contributed towards the observed asymmetries.

Electronic drifts: As discussed in Chapter 2, the possibility of long-term drifts in electronic equipment was specifically taken into account in the design of the experiment. The mobile detector alternated automatically between the 30° and the 180° configurations every few minutes. The effect of long-term electronic drifts would thus be evenly distributed between the 30° and 180° measurements.

Cross-talk: The shadow shield of borated wax between the liquid scintillators in the 30° configuration would have attenuated most

of the neutrons scattered from one detector towards the other (Pr77). Since the detectors were equal distances from the source, a neutron would either have to be scattered at an angle close to 90° or be scattered twice in order to reach one detector from the other. In either case, one would expect the majority of such scattered neutrons to fall below the neutron energy detection threshold, particularly in the case of Run 3, for which the threshold was as high as 975 keV. In any case, the expected asymmetrical effect of this cross-talk is opposite to that which was observed: the additional low-energy neutrons in the 30° configuration measurements would, because of the Maxwellian shape of the spectrum (more events in the lower-energy portion of the distribution), result in the energy distributions at 30° being less dispersed than those at 180°, contrary to the implications of the observed asymmetries.

The effect of neutron scattering directly from the wax into one of the liquid scintillators has, of course, been allowed for in the placing of a "dummy" wax shadow shield at the 180° position. Cross-talk effects or asymmetrical scattering from the wax are consequently not considered to be responsible for the observed asymmetries.

Accidental counts: The probability of detecting two neutrons in coincidence at 180° (mostly from opposite fragments) is greater than the probability of detecting two coincident neutrons at 30°, for two reasons. Firstly, the angular distribution of neutrons in the laboratory frame is forward-peaked, relative to the fission axis; with the detectors at 180°, there would, for instance, be times when the fission axis points directly towards both detectors (favouring neutron detection), which obviously can never occur when they are in the 30°

configuration. Secondly, at 180°, coincident neutron events will sometimes be recorded in which one or both of the fission fragments have emitted *only* one neutron. This can only happen at 30° for the rare cases in which the coincident neutrons do not originate from the same fragment. Further implications of this observation will be discussed below. A comparison of the total number of coincidence events recorded at each configuration, during equal run times (see Section 3.2), illustrates the discrepancies in neutron count rates: there were 23% more coincident neutron events recorded at 180° than at 30° during Run 3, and 10% more during Run 4, the difference in these figures being presumably due to the different energy thresholds for each Run.

However, over equal run times, the number of *accidental* coincidences recorded at each configuration would be expected to be essentially the same, so that the 30° configuration data would contain a higher proportion of accidental counts than the 180° configuration data. The presence of accidentals causes the largest perturbations in the high-energy region of the spectra, where the intensity of "real" events is low. The observed asymmetries could thus be caused by the greater proportion of accidental counts in the high-energy region of the 30° configuration data, which could result in these energy distributions being more dispersed (less correlated) than those formed from the 180° configuration data.

Neutron Multiplicity: The average neutron multiplicity for the spontaneous fission of ^{252}Cf is $\sim$3,8 neutrons per fission (Sp82, Ma82), that is slightly under two per fragment. The strong saw-tooth dependancy of neutron yield on fragment mass is illustrated in Figure 4.1.

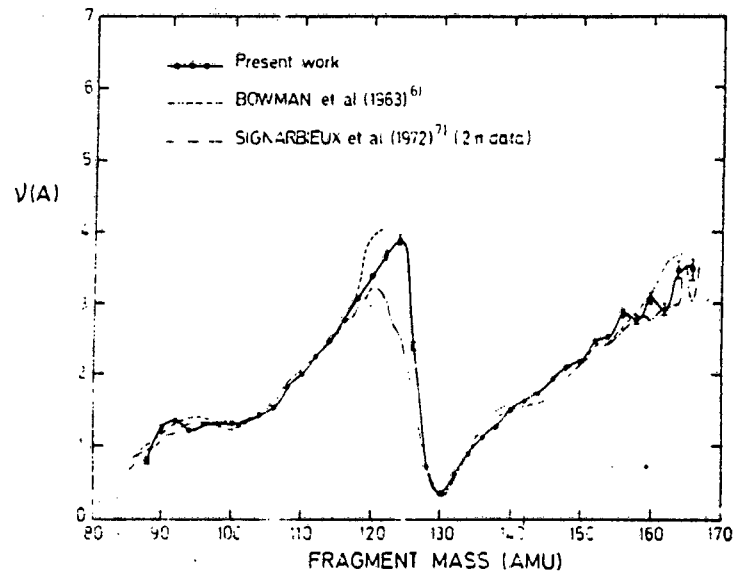

Figure 4.1: Measured average neutron yield as a function of fragment mass. (Figure from Wa77).

It can be seen that, for a substantial number of fragment masses, including some of those which are highly favoured by the "double-humped" mass yield (see Figure 3.11), the average neutron yield is somewhat less than two per fragment. As was pointed out in the discussion on accidental counts, more coincident events in which one or both fragments emit only one neutron would be recorded at 180° than at 30°. Terrell (Te57) has shown that the average initial excitation energy of a fission fragment, E_x, is related to the average neutron multiplicity, $\bar{\nu}$, for the particular mass split, by the simple relationship:

$$E_x = C_1 (\bar{\nu} + 1)$$

where C_1 is a constant related to the excitation energy change per emitted neutron. This relationship provides the means of expressing the average neutron energy, $\bar{E}$, in terms of $\bar{\nu}$, since:

(a) in the Weisskopf statistical picture (We37), in which the excited nucleus is analogous to a degenerate Fermi gas, the approximate thermodynamic relationship between E_x and the nuclear temperature, T, is:

$E_x = aT^2$, where a is a constant; and

(b) for an evaporation spectrum of the Maxwellian form, the average neutron energy, $\bar{E}$, is related to the nuclear temperature by the simple formula (Te59), $\bar{E} = 3T/2$.

The combination of these relationships yields, for the average centre-of-mass neutron energy emitted by a fragment of mass A:

$\bar{E}(A) = C_2(\bar{\nu}(A) + 1)^{\frac{1}{2}}$, where C_2 is a constant.

According to this relationship, the average neutron energy is higher when more than one neutron is emitted by a fragment than when only one neutron is emitted, from which it may be inferred that, when the detectors in this experiment were in the 180° configuration, the energy distributions of the observed neutrons would have been further biased towards the low-energy region than when they were in the 30° configuration; because of the Maxwellian shape of the spectrum, these distributions would, therefore, have been less dispersed in energy, which is another possible explanation for the higher correlation observed for data measured at 180°, even for non-coincidental neutrons.

However, the validity of Terrell's relationship for $T(\bar{\nu})$, when it is applied to different mass splits of the same fissioning nucleus,

has been questioned (Bo63, K172). Bowman and co-workers (Bo63) measured the average centre-of-mass kinetic energy of the neutrons, $\bar{\eta}$, as a function of fragment mass, and revealed the surprising fact that, whereas the saw-tooth shape of the neutron multiplicity distribution is very asymmetric with respect to mass 126, the "half-way" mass number for ^{252}Cf (see Figure 4.1), the distribution of $\bar{\eta}(A)$ is nearly symmetric with respect to this mass. Figure 4.2 is a composite representation of (i) the measured $\bar{\eta}(A)$ distribution; (ii) the mass yield results of Walsh and Boldeman (Wa77); and (iii) regions representing different values of the neutron multiplicity $\bar{\nu}(A)$.

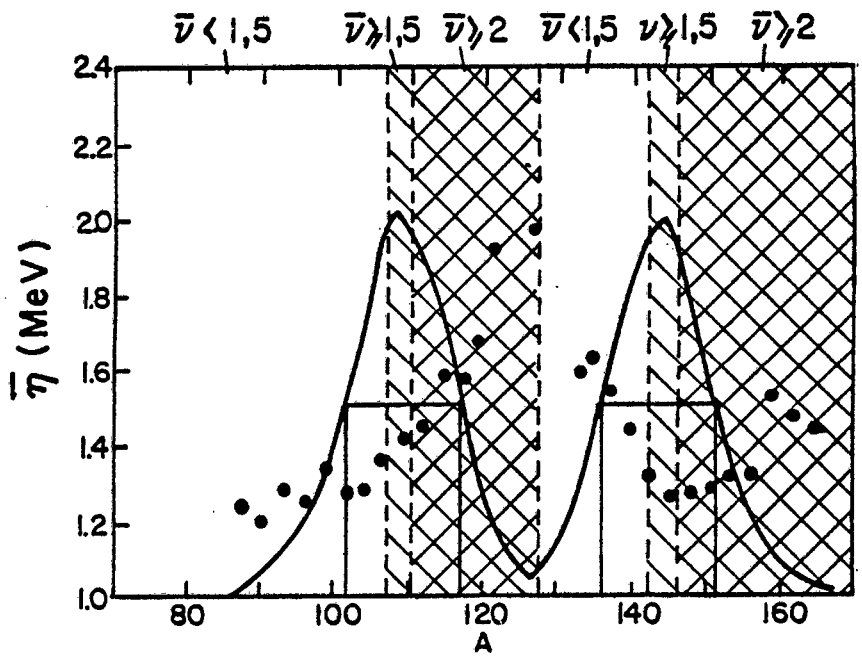

Figure 4.2: The average centre-of-mass neutron energy as a function of fragment mass (Bo63) is represented by the dots. Also shown is the mass yield distribution (arbitrary vertical scale) measured by Walsh and Boldeman (Wa77). The solid lines represent the FWHM region of the peaks. The average number of neutrons per fragment is indicated broadly by three groupings: $\bar{\nu}$ <1,5 (unhatched areas); $\bar{\nu} \geq 1,5$ (hatched areas); and $\bar{\nu} \geq 2$ (cross-hatched areas).

Most of the light fragments fall within the mass range defined by the Full Width at Half Maximum of the mass yield distribution, that is 102 - 117 a.m.u. Over this range, both the average centre-of-mass neutron energy and the neutron multiplicity increase with increasing mass number. However, the opposite is true over the range of predominant heavy fragment masses, 136 - 151 a.m.u. The average energy of neutrons emitted by fragments around mass 136, where the average number of neutrons per fragment is <1,5, is higher than in the region of mass 148, where the corresponding number of neutrons per fragment is >2. Gavron and Fraenkel (Ga74) measured a distribution of $\bar{n}(A)$ which was essentially the same as that of Bowman *et al.* They also found that the average centre-of-mass neutron energy was the same for events in which they measured only one neutron, or two neutrons respectively.

The results indicate that Terrell's $T(\bar{\nu})$ relationship should be used only as a rough general guide. The discrepancies, in this experiment, between the neutron energy distributions measured in the 180° and 30° configurations respectively are unlikely to have been caused *solely* as a result of the difference in average neutron multiplicities. Nevertheless, this systematic imbalance may have contributed towards the observed asymmetries.

To summarise, the observed systematic experimental asymmetries in non-coincidental neutron energies may be due to a combination of two effects, namely the higher proportion of accidental counts (particularly important in the high-energy region) recorded at 30°, and the different neutron multiplicity constraints on the detection of coincident neutrons at 180° and 30° respectively.

4.3 CORRELATIONS OF COINCIDENT NEUTRON ENERGIES

There are two questions which need to be answered with respect to the *coincident* neutron energy data:

(1) Why are the coincident neutron energies more strongly correlated than the non-coincident neutron energies at both 30° and 180°?

(2) Is there enough evidence for the cascade effect on the energies of coincident neutrons from the fact that the 30° configuration energies are less correlated than the 180° configuration energies?

The critical factor in the evaluation of the second question is the fact that the non-coincidental data also exhibit different degrees of correlation at 30° and at 180° respectively; it was illustrated in Table 3.4 that the differences Δr between the 180° and 30° linear correlation coefficients are similar for the coincident and non-coincident neutron energy pairs. Thus, it is not necessarily true that the difference Δr between the correlation coefficients determined for coincident neutrons is a manifestation of the cascade cooling (anti-correlation) effect.

On the other hand, the factors which contribute towards asymmetries in the non-coincidental neutron energy correlations may have little in common with those which cause the asymmetries in coincident neutron energy correlations.

Possible causes of asymmetries in the *coincident* neutron energy correlations are discussed in the next four sections.

4.4 KINEMATICS

The raw data acquired in this experiment consist of the times-of-flight of coincident prompt fission neutrons, which yield their velocities (and thus energies) in the *laboratory* frame of reference. The velocity of a neutron in the laboratory frame is the vector resultant of its centre-of-mass velocity and the velocity of the parent fragment. For a neutron emitted from a moving fragment at a centre-of-mass angle $\phi_{c.m.}$ (relative to the fission axis), the relationship between the laboratory energy E and the centre-of-mass energy $E_{c.m.}$ is given by (Te59)

$$E = E_f + E_{c.m.} + 2(E_f E_{c.m.})^{\frac{1}{2}} \cos\phi_{c.m.} \qquad (4.1)$$

where E_f is the energy of a neutron moving with the velocity of the fragment. The interesting physics with regard to nuclear temperature and the cascade cooling effect lies in the values of $E_{c.m.}$, which cannot be determined independently since the fission fragments themselves were not detected in this experiment. The distributions of the laboratory energies E thus yield a "blurred" view of the information on the evaporation process conveyed by the centre-of-mass energy distributions ($E_{c.m.}$). However, in this experiment, several thousand pairs of coincident neutron energies were recorded in each configuration; general trends in the centre-of-mass energy distributions should thus be noticeable in the distributions of laboratory energies.

Since the significance of the results of this experiment depend upon the interpretation of the *difference* in neutron-neutron energy corre-

lations measured at 30° and 180° respectively, it is important to determine whether or not these two geometries produce *asymmetric* kinematic effects on the coincident neutron energies. Qualitative answers to this question may be found with relative ease, if a few approximations are used (a more rigorous treatment would require a laborious modelling procedure, such as a Monte Carlo simulation).

Figure 4.3 shows the relationships between the various velocities and angles involved in the emission of a neutron from a moving fragment.

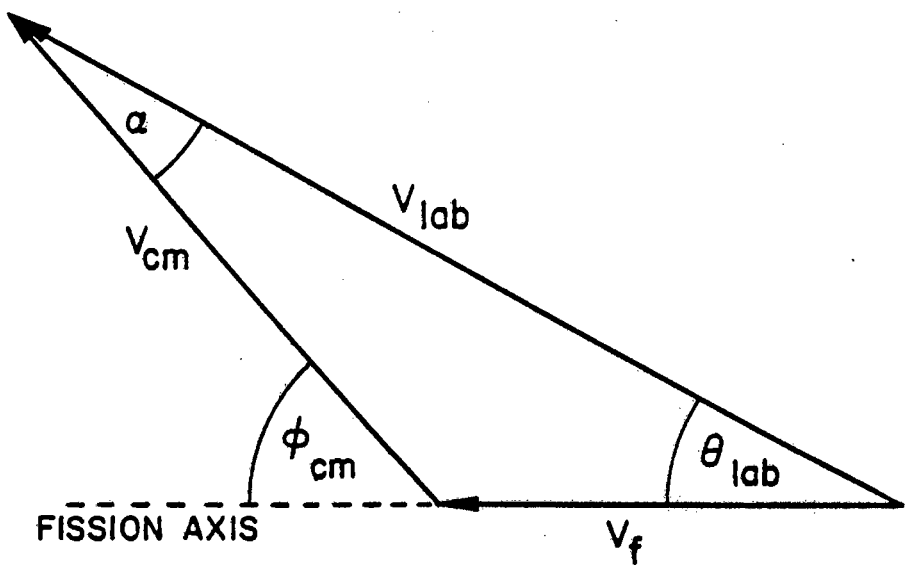

Figure 4.3: Schematic illustration of the kinematics. The laboratory velocity v_{lab} of a neutron detected at angle θ_{lab} to the fission axis, is the resultant of the fragment velocity v_f and the neutron centre-of-mass velocity $v_{c.m.}$. The neutron is emitted at angle $\phi_{c.m.}$ to the fission axis in the reference frame of the fragment.

The trigonometric Law of Sines gives

$$\frac{v_{c.m.}}{\text{Sin } \theta_{lab}} = \frac{v_f}{\text{Sin}\alpha}$$

$$\therefore \quad \alpha = \text{Sin}^{-1}((v_f/v_{c.m.})\text{Sin } \theta_{lab})$$

and, since $\phi_{c.m.} = \alpha + \theta_{lab}$,

$$\phi_{c.m.} = ((v_f/v_{c.m.})\text{Sin } \theta_{lab}) + \theta_{lab}$$

Consider, firstly, the 180° configuration:
From the angular distribution of neutrons (Figure 1.5) it is obvious that the detection of two coincident neutrons is the most probable when the orientation of the fission axis is along the (0°, 180°) line, that is aligned with the detectors. Equation (4.1) thus reduces to

$$E = E_f + E_{c.m.} + 2(E_f E_{c.m.})^{\frac{1}{2}} \qquad (4.2)$$

The average value of $E_{c.m.}$ is 1,44 MeV (Bo62). Since one neutron from each fragment is detected, two average values of E_f must be considered: the average velocity $\bar{v}_{fL}$ of the light fragments is 1,37 cm/ns (Bo63, Wh63) which results in $\bar{E}_{fL}$ = 0,97 MeV; the corresponding values for the heavy fragment group are $\bar{v}_{fH}$ = 1,04 cm/ns and $\bar{E}_{fH}$ = 0,56 MeV. Thus, if $\bar{E}_L$ and $\bar{E}_H$ represent the average laboratory energies of two neutrons detected in the 180° configuration, with the fission axis pointing towards the detectors,

$$\bar{E}_L = 4{,}78 \text{ MeV}$$

and $\bar{E}_H = 3{,}80$ MeV, by Equation (4.2).

The average difference between the energies, $\bar{E}_L - \bar{E}_H$, is 0,98 Mev. Since Bowman *et al.* (Bo62) have reported that the average centre-of-mass neutron energies are symmetrical about mass 126 (see Figure 4.2), the average centre-of-mass neutron energy $\bar{E}_{c.m.}$ has been assumed to be the same for the light and heavy fragments respectively.

These calculations were repeated for $\theta_{lab} = 15°$ ($\phi_{c.m.} = 27{,}2°$ and 24,3° for the light and heavy fragments respectively). The average neutron energies at this angle are:

$$\bar{E}_L = 4{,}52 \text{ MeV}$$

$$\bar{E}_H = 3{,}64 \text{ MeV}$$

$$\bar{E}_L - \bar{E}_H = 0{,}88 \text{ MeV}$$

Now, the probability of detecting a pair of coincident neutrons when the fission axis is 15° "skew", P(15°, 15°), is about 0,77 of the probability at 0°, P(0°, 0°), according to an estimate based upon the angular distribution of ^{252}Cf neutrons (Figure 4.2). By combining the average neutron energies calculated for 0° and 15° respectively, using the probability ratio as a weighting factor, the result is a rough estimate of the average neutron energy difference caused by the kinematics over the 0° to 15° range of fission axis orientations:

$$\bar{E}_L - \bar{E}_H = 0{,}94 \text{ MeV} \qquad (\theta_{lab} = 0° \text{ to } 15°)$$

This value represents a significant kinematic effect over the 0° to 15° range of fission axis orientations. At larger angles, the magnitude of the effect decreases, but so do the relative number of coincident neutrons reaching the detectors. For example, at an angle of 40°,

$$\bar{E}_L - \bar{E}_H = 0{,}19 \text{ MeV, but } \frac{P(40°, 40°)}{P(0°, 0°)} \text{ is only } 0{,}27.$$

A similar analysis was performed for the 30° configuration: The most important difference, from the kinematic point of view, is that, at 30°, the coincident neutrons originate from the same fission fragment, so that the term E_f is the same in the equation for the laboratory energy of each neutron, Equation (4.1). The other difference is that θ_{lab} is asymmetric with respect to the detectors, except for the special case when the fission axis lies exactly half-way between them, at 15° to each. It is at this orientation that the probability of detection of a coincident neutron pair is greatest; the probability is smaller when the fission axis points directly towards one detector and is at an angle of 30° to the other:

$$\frac{P(-15°, 15°)}{P(0°, 0°)} = 0{,}77; \qquad \frac{P(0°, 30°)}{P(0°, 0°)} = 0{,}63$$

In contrast to the case for the 180° configuration, for which θ_{lab} is always symmetric, but for which kinematic asymmetries arise from the fact that one neutron is emitted by the light fragment and the other is emitted by the slower, heavy fragment, the average energy $\bar{E}_{lab}$ measured in the 30° configuration is the same for both detectors, if one assumes $\bar{E}_{1,c.m.} = \bar{E}_{2,c.m.}$ and if the fission axis points half-way between them.

The effect of different orientations of the fission axis may be assessed in a similar manner to that employed for the 180° case, assuming once again an average centre-of-mass neutron energy, $E_{c.m.}$ = 1,44 MeV, and an overall average fragment velocity $\bar{v}_f$ = 1,20 cm/ns (Bo63, Wh63), which gives $\bar{E}_f$ = 0,746 MeV. The average coincident neutron laboratory energies are designated $\bar{E}_1$ (for the detector at the 0° position) and $\bar{E}_2$ (for the detector at the 30° position). Then, for symmetric θ_{lab} = (-15°, 15°), $\bar{E}_1 = \bar{E}_2$ = 4,05 MeV.

The corresponding average energies when θ_{lab} = (0°, 30°) are:

$\bar{E}_1$ = 4,26 MeV, and

$\bar{E}_2$ = 3,49 MeV

The average difference is thus $\bar{E}_1 - \bar{E}_2$ = 0,77 MeV.

By a similar process to that outlined for the 180° configuration case, using the probability ratio as a weighting factor, the average neutron energy difference between $\bar{E}_1$ and $\bar{E}_2$ caused by the kinematics over the 0° to 15° range of fission axis orientations is:

$\bar{E}_1 - \bar{E}_2$ = 0,33 MeV

As the angle between the fission axis and the symmetric angle (15°) increases, the difference between $\bar{E}_1$ and $\bar{E}_2$ *also increases*, which is opposite to the trend in the 180° case. However, the probability

of detecting two coincident neutrons decreases, as for the 180° case. For example, at 40° to the symmetric angle, that is θ_{lab} = (25°, 55°),

$$\bar{E}_1 - \bar{E}_2 = 1{,}6 \text{ MeV, but } \frac{P(25°, 55°)}{P(0°, 0°)} \text{ is only } 0{,}21.$$

Figure 4.4 illustrates these results schematically, and, for the sake of easy comparison, they are summarised in Table 4.1.

The kinematic effect on the coincident neutron energies measured at 30° is of a different nature from that which influences the 180° measurements. At 30°, the differences in θ_{lab} of the neutrons entering each detector causes a difference $\Delta\bar{E}$ in their average laboratory energies which increases as the fission axis moves further from the symmetric orientation, where the difference is zero. For the 180° configuration, however, θ_{lab} is symmetric at all fission axis orientations, but the different velocities of the light and heavy fragments respectively cause a difference $\Delta\bar{E}$ in the average neutron energies, which is greatest when the fission axis is aligned with the detectors, and *decreases* as it moves further away from this orientation.

It is difficult to be certain about which of these effects has the larger influence on the measurements, without proceeding to a full Monte Carlo simulation of the experiment, but it seems likely that it would be the "light-heavy" fragment velocity effect on the 180° measurements, since $\Delta\bar{E}$ is greatest when the fission axis is at *small* angles to the detectors, and the probability of coincident neutron detection is consequently relatively high. If this assumption is correct, one might expect a lower correlation of the neutron energy

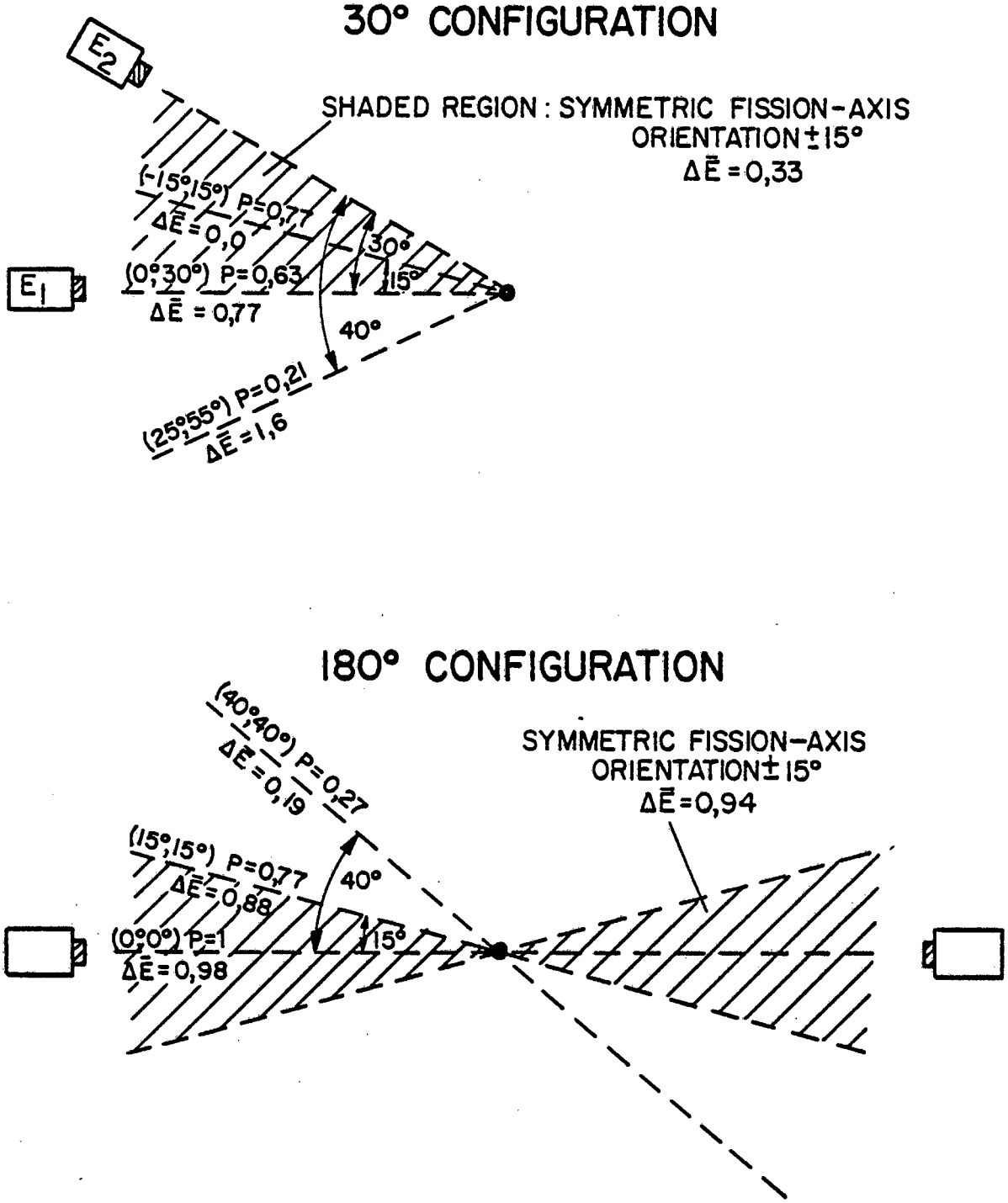

Figure 4.4: Schematic illustration of the kinematic effect of various orientations of the fission axis on the average laboratory energies of coincident neutrons.

TABLE 4.1: A comparison of kinematic effects on the average laboratory energies of coincident neutrons measured in the 30° and 180° configurations respectively

30° CONFIGURATION			180° CONFIGURATION		
θ_{lab1}, θ_{lab2}	$\frac{P(\theta_{lab1}, \theta_{lab2})}{P(0°, 0°)}$	$\Delta\bar{E} = \bar{E}_1 - \bar{E}_2$ (MeV)	θ_{lab1}, θ_{lab2}	$\frac{P(\theta_{lab1}, \theta_{lab2})}{P(0°, 0°)}$	$\Delta\bar{E} = \bar{E}_L - \bar{E}_H$ (MeV)
-15°, 15° (Symmetric orientation)	0,77	0,00	0°, 0°	1	0,98
Average over region (-15°, 15°) ± 15°	-	0,33	Average over region (0°, 0°) ± 15°	-	0,94
0°, 30° (15° from symmetric orientation)	0,63	0,77	15°, 15°	0,77	0,88
25°, 55° (40° from symmetric orientation)	0,21	1,60	40°, 40°	0,27	0,19

pairs measured at 180° than at 30°, from kinematic considerations alone. In fact, the opposite was found, which implies that either:

(a) the above assumption is incorrect; or

(b) other features of neutron emission decrease the correlation of those measured at 30°. The cascade cooling effect on the energies of neutrons from the same fragment is a plausible explanation.

In general, the predicted kinematic effects would enhance the correlation of all *coincident* neutron energy pairs with respect to pairs of *non-coincident* neutron energies. This is one possible explanation for the observation that, whether one considers the measurements at 30° or at 180°, coincident neutrons (from the same *fission* and thus the same fission-axis orientation) are more strongly energy-correlated than are the randomised non-coincident neutrons.

4.5 CENTRE-OF-MASS NEUTRON ENERGIES

For the above discussion of kinematic effects on the laboratory energies of prompt neutrons, the calculations were simplified by the use of *average* centre-of-mass neutron energies. In this section, the factors which determine the centre-of-mass neutron energies, and their relevance to this experiment, will be discussed.

The total energy released in the spontaneous fission of a heavy nucleus such as ^{252}Cf can be expressed simply as the difference between the mass of the fissioning nucleus and the sum of the

masses of the product fragments (Ni74). The amount of total energy released has been shown (Ni74) to vary with the distribution of charge between the fragments, because of proton pairing energy considerations. After scission, this energy takes the form of the sum of the kinetic energies and the internal excitation energies of the fragments. The division of the total energy between the two fragments, and between the kinetic energy and internal excitation energy of a particular fragment, is influenced by shell effects on the deformation of the nascent fragments in the cold transition nucleus (Bo56, Mo71, Wi76).

The initial excitation energy of a fragment of mass A is drawn from an approximately Gaussian distribution (Te57), if it is uncorrelated with the energy of its sister fragment, which, according to the findings of Gavron and Fraenkel (Ga73) and Signarbieux *et al.* (Si74), is indeed the case.

From the fact that the lighter of the two fission fragments emits, on average, more neutrons than the heavier fragment, Bowman *et al.* (Bo62) deduced that the light fragment should possess more initial excitation energy than the heavy fragment, but could find no evidence for this from their measurements of neutron energies: the energy spectra of neutrons from the light and heavy fragments respectively were found to be virtually identical. Even more surprising was the discovery that the average centre-of-mass neutron energy as a function of mass $\bar{\eta}(A)$ is nearly symmetric with respect to mass 126 (see Figure 4.2), whereas the neutron multiplicity function $\bar{\nu}(A)$ is very asymmetric (see Figure 4.1). Since $\bar{\nu}(A)$ gives an indication of the initial excitation energy and $\bar{\eta}(A)$ is

related to nuclear temperature, Bowman and co-workers were *"led to ascribe very different heat capacities to fragments around mass 120 and those around mass 132; the ratios of excitation energies necessary to produce the same temperature in the two regions are of the order of 4 to 1, or more."* Nevertheless, Lang (La64) and, more recently, Nardi *et al.* (Na73) have shown that the standard evaporation theory still accounts satisfactorily for the neutron energy spectra, provided the level densities used in the calculation properly include shell effects. In the neighbourhood of closed shells, such as around mass 133, very low effective specific heats are to be expected. Figure 4.5 illustrates how the nuclear temperature associated with a given excitation energy varies as a function of mass number, peaking around masss 133.

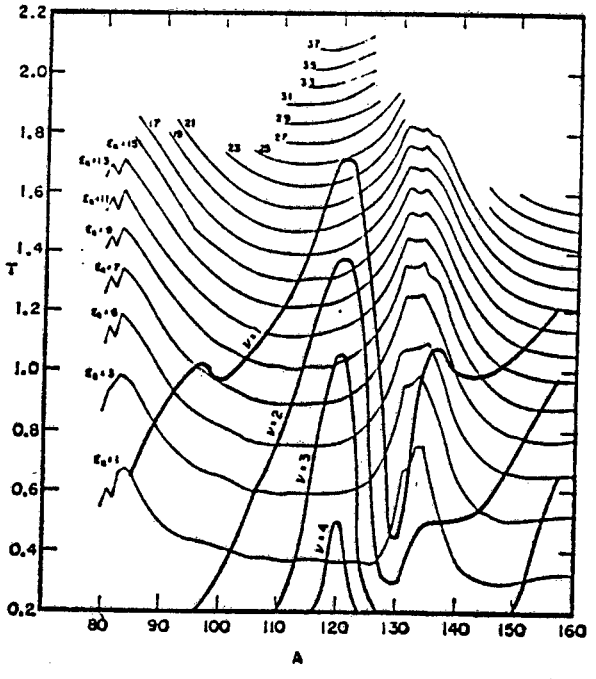

Figure 4.5: The dependance of nuclear temperature T on both excitation energy E_x and fragment mass A. The heavy lines indicate the average temperature after the emission of 1, 2, 3, or 4 neutrons. (Figure from Bo63).

On the basis of present knowledge, it is thus possible to reconcile the symmetric function $\bar{n}(A)$ with the saw-tooth shape of $\bar{\nu}(A)$.

The symmetry of $\bar{n}(A)$ about mass number 126, which is the symmetric *mass* number, implies that the average neutron energies of two fragments from the same fission are roughly equal. Coincident neutron energy pairs might thus be expected to be more correlated than non-coincident pairs, even when the neutrons are emitted by opposite fragments, which could explain the greater energy-energy correlation of coincident neutrons measured at 180° in this experiment. Notwithstanding any anti-correlation effect of the cascade cooling phenomenon, coincident neutrons from the *same* fragment (30° configuration measurements) at least have in common the initial excitation energy of the fragment, which is not the case for non-coincident neutron pairs. The observed overall difference in the degree of correlation between coincident and non-coincident neutron energy pairs respectively could thus be explained in terms of the spread in initial excitation energies and nuclear temperatures of the fission fragments.

Centre-of-mass neutron energy considerations may also be invoked to explain the greater correlation of coincident neutrons measured in the 180° configuration with respect to those measured in the 30° configuration. Consider a fission event for which the average centre-of-mass neutron energies of fragment 1 and fragment 2 are equal, a reasonable assumption in the light of the symmetry of $\bar{n}(A)$ about mass 126. For simplicity, let each fragment emit two neutrons and assume further that the first neutrons from each fragment, "a", are more energetic than the second neutrons, "b", since they are evaporated in a cascade cooling process:

$n_{1a} \approx n_{2a}$, $n_{1b} \approx n_{2b}$;

$n_{1a} > n_{1b}$, $n_{2a} > n_{2b}$

Now, a measurement at 180° of coincident neutrons from this event might be expected to record any one of the following pairs of neutrons, from opposite fragments:

$(n_{1a};n_{2a})$, $(n_{1b};n_{2b})$ - correlated energies

$(n_{1a};n_{2b})$, $(n_{1b};n_{2a})$ - uncorrelated energies

On the other hand, a measurement at 30° would record the energies of a pair of neutrons from the same fragment: $(n_{1a};n_{1b})$ or $(n_{2a};n_{2b})$.

Both of these pairs are uncorrelated (or even anti-correlated). Thus, the overall effect of the emission of prompt neutrons in an evaporation cascade might be expected to be that neutron energy pairs measured at 180° would be more correlated than those measured at 30°, which is in agreement with the calculated linear correlation coefficients (Method B): $r_{180} - r_{30} = 0,047 \pm 0,017$ for coincident neutron energies.

4.6 GAMMA RAY EMISSION AND ANGULAR MOMENTUM

The emission of prompt gamma rays accounts for an average 3,5 Mev (Sk80) of the excitation energy of each fragment and most ($\sim$5-7$\hbar$) of the angular momentum (Ni74). Neutron emission does not remove

much of the initial fragment angular momentum (Jo64), so that γ-emission starts to compete favourably with neutron emission as the cooling fragment approaches the so-called yrast line, which is the locus of lowest energy levels for particular angular momenta (Sp66, Gr67, Th67, Th68), and which thus defines an angular momentum barrier to further neutron emission. The total γ-ray yield versus fragment mass resembles the neutron yield saw-tooth (Jo69) and is thought to be (Ni74) a consequence of the correlation between fragment angular momentum and internal excitation energy.

It is possible that γ-ray emission might even commence before neutron emission is completed, but no positive evidence has yet been found to support this theory (Sk77). It has been suggested (Sa76) that deviations from the normal evaporation distribution may occur in the spectrum of "last" neutrons, emitted by fragments which have cooled to the neighbourhood of the yrast line. However, these small perturbations of the evaporation spectrum would not be expected to be significant in the context of the present investigation.

The angular momenta of the fission fragments are aligned (antiparallel) and directed perpendicular to the fission axis (Wi72, Wo76), which may account for a very small proportion (<2%) of the observed anisotropy in the angular distribution of neutrons (Fr75, Pi78). However, the effect of fragment spin on the *energy* distribution of prompt neutrons is thought to be neglibible (Ni74).

It is thus concluded that γ-ray emission and fragment angular momentum had no significant effect on the coincident neutron energies measured in this experiment.

4.7 ACCIDENTAL COINCIDENCES

The effect of accidental counts on the correlation of non-coincident neutron energy pairs has been discussed in Section 4.2. It was pointed out then that the measurements at 30° would contain a higher proportion of accidental coincidences than those at 180°. This imbalance is also expected to have an influence on the overall correlation of *coincident* neutron energy pairs measured at 30° and at 180° respectively. Neutron energy pairs in which one or both of the energies arise from accidental counts would, on average, be uncorrelated. Since an overall positive correlation of coincident neutron energies is found from measurements at both 30° and 180°, and since the 30° configuration data contain a higher proportion of accidental coincidences, the linear correlation coefficient for 30° neutron energy pairs might be expected to be lower than that for 180° neutron energy pairs, all else being equal. Thus, the observed difference (r_{180} = 0,165; r_{30} = 0,118) could be partially explained by the imbalance in the proportion of accidental coincidences recorded in the 30° and 180° configurations respectively. However, it seems unlikely that <4% of such coincidences in Run 3 and <9% in Run 4 could be the only cause of the differences between r_{180} and r_{30}.

4.8 CONCLUSIONS

The aim of this experiment was to test the "cascade cooling" hypothesis by comparing the energy correlations of coincident neutrons emitted by the same fragment with the correlations of coincident neutrons emitted by opposite fragments. The results may be summarised as follows:

(a) The laboratory energies of coincident neutrons are positively correlated whether they are emitted by the same fragment or by opposite fragments in the same fission event.

(b) The energies of coincident neutrons from the same fragment are less correlated than those from opposite fragments.

(c) The energies of non-coincidental neutrons are also correlated, but significantly less so than the energies of coincident neutrons.

(d) Non-coincidental neutron energy pairs formed from measurements in the 30° configuration (coincident neutrons from the same fragment) are less correlated than pairs formed from measurements in the 180° configuration (coincident neutrons from opposite fragments).

(e) The *differences* between the correlations measured at 30° (same fragment) and at 180° (opposite fragments) respectively, are similar for coincident and non-coincident neutron energy pairs.

The most likely explanations for the difference in correlation of non-coincident neutron energies from 30° and 180° measurements respectively, are (i) the higher proportion of accidental counts in the 30° configuration, and (ii) the fact that the number of neutrons per fragment ν is always >1 for measurements at 30°, but can be equal to one for measurements at 180°. Plausible as these explanations may be, it is puzzling that the effects should so noticeable, since the proportion of accidental counts is small, and it has been shown that the average neutron energies are similar for $\nu = 1$ and $\nu > 1$ respectively. It is possible that some other source of asymmetry which has not been considered, is in evidence here.

For the case of the *coincident* neutron energies, the larger overall correlations with respect to non-coincidental energies can be adequately ascribed to kinematic effects and to the spread in initial fragment excitation energies.

The energy correlation effect of the kinematics is likely to be stronger on neutrons measured at 30° than on those measured at 180°. It has been found, however, that coincident neutrons from the same fragment are less energy-correlated than those from opposite fragments in the same fission. This agrees with the predicted effect of the cascade cooling phenomenon which would thus appear to be pronounced enough to counteract the kinematic effect on the energy correlations. The imbalance of accidental coincidences between the two configurations could also be a contributory factor to this result.

Within the limitations imposed by the design of this experiment, then, it can be tentatively claimed that evidence has been found for the cascade cooling of excited fission fragments during the evaporation of prompt neutrons. The stumbling block which prohibits a more clear-cut result is the difference in correlation of non-coincident neutron energies measured in the two experimental configurations. Unless this difference can be satisfactorily explained in terms of factors which do not affect the coincident neutron energy distributions, some uncertainty must remain with regard to the above conclusions.

The best way to assess the relative magnitudes of all the factors which influence these correlation results would be to proceed to a full Monte Carlo simulation of this experiment.

4.9 FURTHER WORK

There are several improvements which could be made to the experiment without changing the basic design. Firstly, the efficiencies of the detectors could be improved. Since angular resolution is not important in this experiment, larger liquid scintillators could be used for the detection of the neutrons. Of course, if they are thicker, energy resolution suffers from the extra uncertainty in the exact length of the flight-path. However, more efficient detectors could sustain the same count rate as those which were used in this experiment, at a further distance from the source, thus *improving* the energy resolution. The efficiency of the plastic-scintillator time-zero detector could also be improved by means of a 4π arrangement, rather than the simple "well" which was used in this experiment.

Such improved efficiencies would allow a higher count rate (improved statistical accuracy of the data) or, if longer flight-paths were used, better energy resolution. The times-of-flight of the neutrons could also be more accurately determined by a proper calculation of the average scattering position in the liquid scintillators, as performed by Bowman *et al.* (Bo62). The distance from the source to the *middle* of the scintillators has been used as an estimate of the flight-path, which introduces a small non-linear error into the determination of neutron energies.

Although the electronics were tuned to minimise "time-walk", which results from the different response of the photomultipliers to different recoil proton energies (pulse heights), time-walk effects

could not be completely eliminated during data acquisition. However, since the pulse heights are amongst the parameters recorded, time-walk effects may be determined and removed off-line, which is another way of improving the energy resolution.

A procedure for removing some of the accidental coincidences from the data was outlined in Chapter 3. It was not implemented because it was feared that the process might introduce spurious asymmetries between the sets of data. However, in view of the fact that the proportions of accidentals in the 30° and 180° configuration data respectively are, in any case, unequal, and that they are thought to perturb the estimates of the "true" correlations of neutron energies, those accidentals which are easily identifiable should rather be removed from the data.

A more direct way of reducing the ratio of accidental coincidences to "real" coincidences is by reducing the source strength, since the "real" coincidence count rate is proportional to the source strength, whereas the accidental coincidence count rate is proportional to the *square* of the source strength (Yu63). Unfortunately, proportionally longer run times would then be necessary to accumulate the same number of coincidence events.

A small change in the geometry of the experiment would make the interpretation of the results much easier: instead of measuring the energies of neutrons from opposite fragments, emitted at a relative angle of 180° to each other, they should be measured at a relative angle of 150°. Neutrons emitted predominantly from opposite fragments would still be measured, but the two con-

figurations would be more symmetrical. The kinematic effects caused by the orientation of the fission axis with respect to the detectors would then be the same for measurements at 30° and at 150° respectively. The only remaining *asymmetry* in the kinematics would then be that which is caused by the different velocities of the light and heavy fragments. Furthermore, the "real" coincident neutron count rates would be equal at 30° and 150° respectively, so that the asymmetrical effect of the accidental coincidences would disappear, since measurements at each angle would record the same proportion of accidentals.

The simplest and most obvious way to assess the value of the results of this experiment and to gain insight into the relative importance of such factors as the kinematics, accidental coincidences, etc., is by means of a modelling procedure. The Monte Carlo method (U147) is ideally suited to this purpose because of the large body of available data for many of the distributions of the fission variables, and because of the statistical nature of fission and fission fragment de-excitation.

The envisaged approach would incorporate most of the elements of the Monte Carlo simulations performed by Pringle and Brooks (Pr75, Pr77) and by Franklyn *et al.* (Fr78); particular attention would have to be given to a suitable choice of the form of the evaporation spectra of fragment neutrons in the rest frame of their parent fragments, since this is crucial for a meaningful comparison of Monte Carlo predictions with observed energy-energy correlations. For instance, the single-component evaporation spectrum which was

used by these authors does not compare well enough with experimentally determined spectra, such as that of Green *et al.* (Gr73), to be acceptable for this application of the Monte Carlo technique. Pringle and Brooks (Pr80) later adopted the three-component prescription of Bowman *et al.* (Bo62), which reproduced the measured spectra more accurately. Such a spectral form could probably be used if the model included adjustable scission neutron and anisotropy parameters.

The simulations performed by a Monte Carlo program of this type may be divided into two distinct parts:

(i) The von Neumann rejection technique (Ca59) is used to select randomly, from known distributions, such parameters as mass number, neutron yield, etc., which define a particular fission event. The various evaporation models and adjustable parameters are then incorporated into the calculation, which results in a predicted set of neutron energies and emission angles for that particular fission event. As many fission histories as are required for good statistical accuracy may be generated. It is at this stage of the simulation that the effect of the cascade cooling phenomenon on the laboratory energies of coincident neutrons may be incorporated. For comparison, two sets of simulated neutron energies would be generated; for one set, it would be assumed that the energies of neutrons from the same fragment were uncorrelated, and for the other set, the effect of cascade cooling would be taken into account. Presumably,

some parameters would have to be adjusted so that the total neutron energy distributions of both sets would reproduce measured distributions.

(ii) In the second stage of the calculations, the experiment itself is simulated. Detector biases, geometries and efficiency functions are all simulated, so that the mock "measurements" should resemble those which were made in the experiment.

The resultant two sets ("cascade" and "no cascade") of coincident neutron energy pairs (each comprising subsets of 30° and 180° data) could then be analysed in the same way as the "real" data and comparisons with the results of the "real" data analysis could be made. As a first check for sensitivity, just the two sets of simulated data could be compared. If no significant differences are found, then either the modelling is inadequate or the cascade cooling phenomenon is actually not detected in the laboratory energy distributions, although the latter seems unlikely. Assuming that the results of the Monte Carlo simulations are indeed sensitive to to the mode of fragment de-excitation, then it would be a simple matter to ascertain which mode (no correlation or cascade correlation) agrees best with the results from the analysis of the "real" data.

It would be easy also to produce simulated non-coincidental neutron energies and even to include accidental coincidences, in order to gain insight into all the experimentally observed effects and to ascertain the relative importance of the factors which are thought to produce them.

REFERENCES

Ad78 J.M. Adams and G. White, Nucl. Instrum. Methods 156 (1978) 459.

Al61 T.K. Alexander and F.S. Goulding, Nucl. Instrum. Methods 13 (1961) 244.

Am72 Technical Bulletin 72/7, Amersham Radiochemical Centre.

Be71 A. Bertin and A. Vitale, Nucl. Instrum. Methods 91 (1971) 649.

Bo39 N. Bohr and J.A. Wheeler, Phys. Rev. 56 (1939) 426.

Bo56 A. Bohr, Int. Conf. Peaceful Uses of Atomic Energy (Proc. Conf. Geneva, 1955) 2, United Nations, New York (1956) 151.

Bo62 H.R. Bowman, S.G. Thompson, J.C.D. Milton and W.J. Swiatecki, Phys. Rev. 126 (1962) 2120.

Bo63 H.R. Bowman, J.C.D. Milton, S.G. Thompson and W.J. Swiatecki, Phys. Rev. 129 (1963) 2133.

Bo74 J.W. Boldeman, Nucl. Sci. Eng. 55 (1974) 188.

Bo79 J.W. Boldeman, D. Culley and R.J. Cawley, Trans. Am. Nucl. Soc. 32 (1979) 733.

Br74 J.C. Browne and F.S. Dietrich, Phys. Rev. C10 (1974) 2545.

Ca59 E.D. Cashwell and C.J. Everett, A Practical Manual on the Monte Carlo Method for Random Walk Problems, Pergamon Press, (1959) New York.

Cr70 R.L. Craun and D.L. Smith, Nucl. Instrum. Methods 80 (1970) 239.

Fe75 N. Feather and D.G. Vass, Commun. R. Soc. Edinburgh (Phys. Sci.) 4 (1975) 47.

Fr75 Z. Fraenkel and I. Mayk, Phys. Rev. C12 (1975) 1809.

Fr78 C.B. Franklyn, C. Hofmeyer and D.W. Mingay, Phys. Lett. 75B (1978) 564.

Ga73 A. Gavron and Z. Fraenkel, Phys. Rev. Lett. 27 (1973) 1148.

Ga74 A. Gavron and Z. Fraenkel, Phys. Rev. C9 (1974) 632.

Ga76 A. Gavron, Phys. Rev. C13 (1976) 2562.

Gr67 J.R. Grover and J. Gilat, Phys. Rev. 157 (1967) 802.

Gr73 L. Green, J.A. Mitchell and N.M. Steen, Nucl. Sci. Eng. 50 (1973) 257

Ha39 O. Hahn and F. Strassmann, Naturwiss 27 (1939) 11.

Jo64 S.A.E. Johansson, Nucl. Phys. 60 (1964) 378.

Jo69 W. John, J.J. Wesolowski and F. Guy, Phys. Lett. 30B (1969) 340.

Ka63 S.S. Kapoor, R. Ramanna and P.N. Rama Rao, Phys. Rev. 131 (1963) 283.

Ki82 M. Kildir and N.K. Aras, Phys. Rev. C25 (1982) 365.

Kl71 Gy. Kluge, Phys. Lett. 37B (1971) 217.

Kl72 Gy. Kluge, in Prompt Fission Neutron Spectra (Proc. Cons. Meeting, Vienna, 1971) IAEA, Vienna (1972) 149.

La64 D.W. Lang, Nucl. Phys. 53 (1964) 113.

Ma82 D.G. Madland and J.R. Nix, Nucl. Sci. Eng. 81 (1982) 213.

Me67 J.W. Meadows, Phys. Rev. 157 (1967) 1076.

Mo71 U. Mosel and H.W. Schmitt, Nucl. Phys. A165 (1971) 73.

Na73 E. Nardi, L.G. Moretto and S.G. Thompson, Phys. Lett. 43B (1973) 259.

Ni74 H. Nifenecker, C. Signarbieux, R. Babinet and J. Poitou, in Physics and Chemistry of Fission (Proc. Symp. Rochester, 1973), 2, IAEA, Vienna (1974) 117.

Pe54 E.S. Pearson and H.O. Hartley, editors, Biometrika Tables for Statisticians, Cambr. Univ. Press, (1954).

Pi78 V.M. Piksajkin, P.P. D'yachenko, G.V. Anikin, E.A. Seregina, G.M. Akhmedov and V.S. Stavinskij, Sov. J. Nucl. Phys. 28(2) (1978) 159.

Pr75 J.S. Pringle and F.D. Brooks, Phys. Rev. Lett. 35 (1975) 1563.

Pr77 J.S. Pringle, Ph.D. thesis, University of Cape Town, (1977).

Pr80 J.S. Pringle and F.D. Brooks, private communication.

Sa76 A.E. Savel'ev, V.P. Gorelov and B.M. Dzyuba, Sov. J. Nucl. Phys. 24 (1976) 135.

Sc66 H.W. Schmitt, J.H. Neiler and F.J. Walter, Phys. Rev. 141 (1966) 1146.

Si72 C. Signarbieux, J. Poitou, M. Ribrag and J. Matuszek, Phys. Lett. 39B (1972) 503.

Si74 C. Signarbieux, R. Babinet, H. Nifenecker and J. Poitou, in Physics and Chemistry of Fission (Proc. Symp. Rochester, 1973), 2, IAEA, Vienna (1974) 179.

Sk63 K. Skarsvåg and K. Bergheim, Nucl. Phys. 45 (1963) 72.

Sk73 K. Skarsvåg, Phys. Scr. 7 (1973) 160.

Sk77 K. Skarsvåg, Phys. Rev. C16 (1977) 1902.

Sk80 K. Skarsvåg, Phys. Rev. C22 (1980) 638.

Sm57 A.B. Smith, P.R. Fields and J.H. Roberts, Phys. Rev. 108 (1957) 411

Sm68 D.L. Smith, R.G. Polk and T.G. Miller, Nucl. Instrum. Methods 64 (1968) 157.

Sp66 D. Sperber, Phys. Rev. 141 (1966) 927.

Sp74 V. Spiegel, Nucl. Sci. Eng. 53 (1974) 326.

Sp82 R.P. Spencer *et al.*, Nucl. Sci. Eng. 80 (1982) 603.

St67 V.M. Strutinsky, Nucl. Phys. A95 (1967) 420.

St68 V.M. Strutinsky, Nucl. Phys. A122 (1968) 1.

Te57 J. Terrell, Phys. Rev. 108 (1957) 783.

Te59 J. Terrell, Phys. Rev. 113 (1959) 527.

Th67 T.D. Thomas and R. Vandenbosch, Phys. Rev. 133B (1964) 976.

Th68 T.D. Thomas, Ann. Rev. Nucl. Sci. 18 (1968) 343.

Ul47 S. Ulam and J. Von Neumann, Bull. Am. Math. Soc. 53 (1947) 1120.

Wa52 B.E. Watt, Phys. Rev. 87 (1952) 1037.

Wa77 R.L. Walsh and J.W. Boldeman, Nucl. Phys. A276 (1977) 189.

We37 V.F. Weisskopf, Phys. Rev. 52 (1937) 295.

We72 H. Werle and H. Bluhm, in Prompt Fission Neutron Spectra (Proc. Cons. Meeting, Vienna, 1971) IAEA, Vienna (1972) 65.

Wh63 S.L. Whetstone, Phys. Rev. 131 (1963) 1232.

Wi72 J.B. Wilhelmy, E. Cheifetz, R.C. Jared, S.G. Thompson, H.R. Bowman and J.O. Rasmussen, Phys. Rev. C5 (1972) 2041

Wi76 B.D. Wilkins, E.P. Steinberg and R.R. Chasman, Phys. Rev. C14 (1976) 1832.

Wo76 A. Wolf and E. Cheifetz, Phys. Rev. C13 (1976) 1952.

Yu63 Yuan, C.L. Luke and W. Chien-Shiung, editors, Methods of Experimental Physics, Vol. 5B (Nuclear Physics), Academic Press, (1963) New York.